International Journal of Engineering Science 221 (2026) 104474

Contents lists available at ScienceDirect

International Journal of Engineering Science

journal homepage: www.elsevier.com/locate/ijengsci

Multiwell phase-field model for arbitrarily strong total-spreading case☆

J. Kozlík [a,c], K. Tůma [b,*], O. Souček [b], J. Dobrzański [c], S. Stupkiewicz [c]

[a] Charles University, Faculty of Mathematics and Physics, Department of Physics of Materials, Ke Karlovu 5, 121 16 Prague, Czech Republic
[b] Charles University, Faculty of Mathematics and Physics, Mathematical Institute, Sokolovská 83, 186 75 Prague, Czech Republic
[c] Institute of Fundamental Technological Research, Polish Academy of Sciences, Pawińskiego 5B, 02-106 Warsaw, Poland

ARTICLE INFO

Dataset link: https://doi.org/10.5281/zenodo.16882290

Dedicated to the memory of Professor K.R. Rajagopal (November 24, 1950–March 20, 2025), whose never-ending pursuit of physically based and mathematically well-posed models of real-world phenomena inspired some of the present authors.

Keywords:
Interfaces
Phase transition
Total-spreading regime
ω phase
Titanium alloys
Phase-field method

ABSTRACT

In this paper, we revisit a classical multiwell phase-field model in the context of β–ω phase transformations in titanium alloys. We propose a novel model by adjusting the algebraic part of the traditional interfacial free energy in a way that allows for a relaxation of the standard well-posedness constraints on surface tensions in the total-spreading case. The proposed adjustment effectively prevents the formation of a mixed ω–ω state in the resulting phase-field continuum model, aligning with the crystallographic impossibility of such a configuration in reality. We further introduce a chemical energy mixing function that preserves the local stability of purely two-phase β–ω configurations, preventing the spontaneous appearance of additional phases. We illustrate the advantages of the novel model through numerical simulations in one, two and three spatial dimensions and outline a pathway toward a more realistic model of β–ω transition model in titanium alloys.

1. Introduction

1.1. Motivation

In materials science, one is often faced with a problem of secondary phase precipitation within a primary matrix. Usually, the secondary phase is found in several orientations called *variants*, all of them being chemically equivalent. Their number and arrangement generally depend on the crystal symmetries of both the matrix and the precipitate. The individual variants may interact not only with the matrix but also among themselves, especially at the end of the process, when they start touching each other. Therefore, multi-phase models are required to investigate such systems.

A particular example (and our primary motivation) are titanium alloys, where a so-called ω phase (hexagonal) can form within the β matrix (cubic), in 4 variants (Banerjee & Mukhopadhyay, 2007); the same applies for zirconium alloys as well. A unique property of the ω phase is that its interface with the β phase is not atomically sharp, but rather diffuse, i.e., the β–ω interface spans

☆ This article is part of a Special issue entitled: 'IJES_Tribute to Rajagopal' published in International Journal of Engineering Science.

* Corresponding author.
E-mail addresses: jiri.kozlik@matfyz.cuni.cz (J. Kozlík), ktuma@karlin.mff.cuni.cz (K. Tůma), ondrej.soucek@mff.cuni.cz (O. Souček), jdobrz@ippt.pan.pl (J. Dobrzański), sstupkie@ippt.pan.pl (S. Stupkiewicz).

https://doi.org/10.1016/j.ijengsci.2026.104474
Received 5 September 2025; Received in revised form 10 January 2026; Accepted 11 January 2026

across several atomic layers (~1 nm) (Devaraj et al., 2012; Šmilauerová et al., 2017; Zheng et al., 2016). This makes the phase-field modeling approach, in which interfaces are considered to be diffuse rather than sharp, particularly suitable for the description of the microstructure containing this phase. Physically, the finite thickness of the β–ω interfaces is associated with a gradual collapse of {111} planes, which is the actual mechanism of the β–ω transformation.

Another special property of the β–ω system is that (unlike in typical martensitic transformations), the direct ω–ω interface is incompatible at the atomic level and the (hypothetical) ω–ω interfaces would have very high interfacial energy. As a result, direct ω–ω interfaces are not observed and ω particles are separated by the parent β phase. This situation is referred to as *total spreading*.

In the "Ti and Zr community", two types of the ω phase are distinguished: at first, a so-called *athermal* ω forms via a diffusionless process, resulting in nano-scale particles up to 5 nm in size (Šmilauerová et al., 2017). Upon heating, diffusion activates and ω particles grow simultaneously with the elemental partitioning. This is usually referred to as *isothermal* ω and the particle size can reach hundreds of nm, depending on the heat treatment. In this paper, we will deal solely with the scenario typical for the *athermal* ω, i.e., one formed by the diffusionless process during quenching.

1.2. Phase-field models for multi-component systems

The phase-field method is a well-established and versatile computational technique used, among other applications, to simulate microstructure evolution in materials (Chen, 2002; Moelans et al., 2008; Singer-Loginova & Singer, 2008; Steinbach, 2009; Wang & Li, 2010), see also the seminal works (Allen & Cahn, 1979; Cahn & Hilliard, 1958), including the mathematical (Caginalp, 1986) and thermodynamic (Heida et al., 2012a, 2012b; Penrose & Fife, 1990) foundations. The method is based on the fundamental concept of a diffuse interface between material phases. Consequently, this region is treated as having a finite thickness, within which there is a continuous, smooth change in physical properties. To this end, an independent scalar field, called the phase field or order parameter, is introduced into the model. This field takes constant values within individual phases, and its continuous change determines the location of the interface between phases. At the same time, the gradient of the phase field is used to introduce the energy of (diffuse) interfaces. The transformation of the phase field is governed by the evolution equation (e.g., the time-dependent Ginzburg–Landau equation for a non-conserved order parameter), which results from the minimization of the total free energy of the system. The substantial versatility of the phase-field method stems from its flexible structure, which may be combined with virtually any physics. This feature has enabled its extensive use in various fields, including solidification (Kobayashi, 1993; Ode et al., 2001), solid-state transformations (Chen, 2002; Levitas & Preston, 2002; Tůma et al., 2021; Ubachs et al., 2004; Wang & Khachaturyan, 1997), fracture (Ambati et al., 2014; Bourdin et al., 2000), ferroelectric (Choudhury et al., 2005; Guin & Kochmann, 2023; Li et al., 2001) and magnetic domain evolution (Zhang & Chen, 2005), biological applications (Biben et al., 2005; Du et al., 2006), and many more.

Standard phase-field method models perform well with two-phase systems where the use of a single order parameter is sufficient. In reality, however, the evolution of the microstructure of many materials involves more than two phases, which necessitated an extension to the existing approach. One of the earliest attempts to address this challenge was made by Chen and Yang (1994) and later by Fan and Chen (1997), who used a continuum diffuse-interface field model to simulate grain growth, employing a large set of independent order parameters governed by the Ginzburg–Landau equations to describe various grain orientations. At the same time, a pioneering contribution established the *multiphase-field method* (Steinbach & Pezzolla, 1999; Steinbach et al., 1996). In this formulation, the sum-to-unity constraint was imposed on the phase fields, thereby giving their values a possible physical interpretation as volume fractions at any point in the domain. The first paper (Steinbach et al., 1996) extended the standard double-well potential for multiphase cases, while the subsequent work (Steinbach & Pezzolla, 1999) introduced a multi-obstacle potential, the two most common forms of interfacial energy used to this day. The importance of considering triple points and higher-order interactions (multiple junctions) was also emphasized, stressing the need for their proper treatment to ensure model consistency.

1.3. Phase-field models for the β–ω transformation

To the best of our knowledge, there is only a limited number of papers modeling the β–ω transformation using the phase-field method. Notably, there are papers dealing with the Zr-Nb alloy (Tang et al., 2012; Yeddu & Lookman, 2015). One of the objectives of these studies was to simulate the experimentally observed ellipsoidal shape of the individual ω particles, which was achieved by incorporating anisotropy in both elasticity and interfacial energy. However, these models suffer from several drawbacks. First, they allow direct contact between two ω variants, which is not physically admissible, as discussed above. And second, supercritical ω nuclei were randomly distributed at the start of the simulation, which is fine for the study of the particle shape, but not desirable for the study of the early formation kinetics. A model for isothermal ω (i.e., formed by a diffusional mechanism) in Zr-Nb alloy was also proposed by Tang et al. (2012), but the direct contact between ω particles was not completely prevented.

Recently, a phase-field model for the β–ω transformation in Ti-19V alloy, taking also diffusion into account, has been proposed (Gao et al., 2025). Therefore, the model is capable of simulating the evolution of isothermal ω (formed during annealing). The model shows no direct contact between different ω variants, but only due to the presence of the V-enriched layer between them (i.e., the contact is not prevented *per se*). Again, explicit nucleation was used with seeds that were 12 nm in diameter. Particles of this size are well beyond the typical sizes observed for the athermal ω (< 5 nm), making the model not useful to simulate the early stages of ω formation.

To describe the phase energy landscape, all of the studies mentioned above use the models with Landau-type polynomials. The coefficients of the polynomial were determined by fitting the available thermodynamic (CALPHAD) data for the selected

temperatures. This model was introduced by Cook (1975) for Zr-Nb system, describing the phase transformation as first-order and suggesting that the plane collapse is not complete in equilibrium. However, more recent ab-initio DFT simulations of the Ti-Nb system (Ehemann & Wilkins, 2017) suggested that the athermal ω transformation is rather of a second-order, having no energy barrier between β and ω, and that the energy minimum is for fully collapsed ω.

1.4. Aim and novelty of the paper

As discussed above, the existing phase-field models are not capable of describing the total-spreading case and thus cannot properly model the phenomena relevant, for instance, for the β–ω transformation in titanium alloys. The aim of this work is thus to develop a model that would prevent direct contact between two ω variants for arbitrarily large driving forces. In this paper, we deliberately limit ourselves to the driving forces originating solely from the chemical energy, as this simplified setting suffices to capture the main phenomena and to devise the corresponding features of the free energy of the system. Extension to a more complete model including elastic interactions and diffusion is the subject of ongoing work and will be published separately.

To achieve the general goal formulated above, we propose two enhancements of the classical multiwell free energy function. We modify the algebraic part of the interfacial energy by adding a new "double-ditch" term that effectively prevents formation of mixed ω–ω states. Secondly, we introduce a chemical energy mixing function, the "elliptic mixing", which preserves the local stability of purely two-phase β–ω configurations, thus preventing undesired appearance of additional phases. The above enhancements are accompanied by a detailed discussion of the total-spreading case, an aspect that seems insufficiently recognized to date.

As a side result, we provide a general and simple derivation of the constraints on the gradient part (capillary matrix) of the interfacial energy of a constrained system. For the problem at hand, we also show, apparently for the first time, the equivalence of the diagonal and off-diagonal forms of the capillary and mobility matrices upon enforcing the sum-to-unity constraint.

The paper is organized as follows. The general variational framework is briefly introduced in Section 2. In Section 3, the classical phase-field model is specified, and the governing equations are formulated in the reduced form which exploits the sum-to-unity constraint. In Section 4, the condition of evolutionary consistency (EC) is formulated and examined for the reference model, and the resulting conditions on the interfacial energy parameters are derived. The chemical energy with the corresponding simple mixing function are introduced into the model in Section 5. In Section 6, the total-spreading case is discussed and the free energy is augmented with the double-ditch term as a means of separating the ω variants. In Section 7, the elliptic mixing of chemical energy is introduced, which is consistent with the EC condition. A rich set of numerical simulations illustrating the features of the model is reported in Section 8. Finally, a discussion of selected aspects and features of the model is provided in Section 9.

1.5. Notation and interpretation remarks

Due to our motivation to model a specific system, we will use the standard nomenclature of Ti alloys. The matrix/parent phase will be denoted as β and corresponding variables will be indexed either with β, or with the index 0 (e.g. the phase-field variable η_0). Analogically, the ith variant of the precipitate/secondary phases will be denoted as ω_i or indexed by the corresponding index (e.g., variable η_i). Despite the convention used in the paper, the problem analysis is valid for many other systems containing multiple secondary phases within a single matrix.

2. General setup: variational formulation

We aim to develop a general thermo-mechano-chemically driven phase-field model for the β–ω phase transformation in titanium alloys. To highlight the novel features of the model, in this paper, we focus exclusively on its phase-field component, other aspects, like elasticity and diffusion, are not discussed.

To this end, we adopt the general variational framework of *standard dissipative solids* (Biot, 1965; Halphen & Nguyen, 1975; Miehe, 2011; Onsager, 1931; Ziegler, 1963) in a setting adopted for multiphase materials (Chen & Yang, 1994; Steinbach et al., 1996). We consider a multiphase material that can exist in $N+1$ distinct phases, each represented by a phase-field variable η_i playing the role of an order parameter,

$$\eta_i \geq 0, \qquad i = 0, \dots, N, \qquad \sum_{i=0}^{N} \eta_i = 1. \tag{1}$$

In the context of the β–ω transformation, each order parameter η_i ($i \geq 1$) can be related to the degree of the collapse of the {111} planes of the corresponding ω_i variant.

For convenience, we collect all order parameters in a composition vector $\boldsymbol{\eta}$ and introduce the following auxiliary vectors of length $N+1$,

$$\boldsymbol{\eta} = (\eta_0, \dots, \eta_N)^{\mathrm{T}}, \qquad \mathbf{1} = (1, \dots, 1)^{\mathrm{T}}, \qquad \mathbf{e}_i = (0, \dots, 0, 1, 0, \dots, 0)^{\mathrm{T}}, \tag{2}$$

such that $\mathbf{1} = \sum_{i=0}^{N} \mathbf{e}_i$.

The evolution of the system is governed by two functionals: the *dissipation (pseudo-)potential* $\mathcal{D}$, which characterizes how the system dissipates energy, and the *Helmholtz free energy* $\mathcal{F}$, which describes how energy is stored in the material. The dissipation

potential is a function of the rates $\dot{\eta}_i$, while the Helmholtz free energy depends on the η_i's and their spatial gradients. The evolution of each phase is then postulated to follow a gradient flow (also known as a Ginzburg–Landau equation), given by

$$\frac{\delta \mathcal{D}(\dot{\boldsymbol{\eta}})}{\delta \dot{\boldsymbol{\eta}}} + \frac{\delta \mathcal{F}(\boldsymbol{\eta})}{\delta \boldsymbol{\eta}} = \mathbf{0}, \tag{3}$$

where the symbol δ denotes the functional (Gâteaux) derivative,

$$\frac{\delta \mathcal{F}}{\delta \boldsymbol{\eta}} = \frac{\partial F}{\partial \boldsymbol{\eta}} - \nabla \cdot \frac{\partial F}{\partial \nabla \boldsymbol{\eta}}, \qquad \mathcal{F} = \int_\Omega F(\boldsymbol{\eta}, \nabla \boldsymbol{\eta}) \, \mathrm{d}X, \tag{4}$$

$$\frac{\delta \mathcal{D}}{\delta \dot{\boldsymbol{\eta}}} = \frac{\partial D}{\partial \dot{\boldsymbol{\eta}}}, \qquad \mathcal{D} = \int_\Omega D(\dot{\boldsymbol{\eta}}) \, \mathrm{d}X. \tag{5}$$

Here, F denotes the free energy density, Ω is the domain occupied by the body, and ∇ denotes the spatial gradient so that $\nabla \boldsymbol{\eta}$ is a matrix of dimension $N \times d$ (d denoting the spatial dimension), i.e., $\nabla \boldsymbol{\eta} = (\nabla \eta_0, \dots, \nabla \eta_N)^{\mathrm{T}}$. Depending on the specific choices of $\mathcal{D}$ and $\mathcal{F}$, one obtains particular forms of the governing equations. We now proceed to outline these model-specific assumptions.

3. Model assumptions and simplifications

In line with standard assumptions in phase-field theory, we assume that each order parameter η_i is a continuous function of both time and spatial coordinates. The Helmholtz free energy is decomposed into a bulk component $\mathcal{F}_{\mathrm{bulk}}$ and an interfacial component $\mathcal{F}_{\mathrm{int}}$, such that

$$\mathcal{F} = \mathcal{F}_{\mathrm{bulk}} + \mathcal{F}_{\mathrm{int}}. \tag{6}$$

In this work, the bulk energy $\mathcal{F}_{\mathrm{bulk}}$ is taken to be the chemical free energy $\mathcal{F}_{\mathrm{chem}}$, although it can be readily extended to include additional contributions such as thermal or elastic energy. These contributions collectively determine which phase is energetically preferred under given conditions.

3.1. Interfacial energy: general structure

For the interfacial energy $\mathcal{F}_{\mathrm{int}}$, two classical forms are widely used and accepted within the phase-field modeling community: the *double-well* potential and the *double-obstacle* potential (Ohno & Matsuura, 2010; Steinbach, 2009). In this work, we adopt the double-well potential, primarily for numerical convenience.

In the case of two phases, we have $\eta_1 = \eta$ and $\eta_0 = 1 - \eta$ from the sum-to-unity constraint $(1)_3$, and the double-well interfacial energy is given by

$$\mathcal{F}_{\mathrm{int}} = \int_\Omega F_{\mathrm{int}}(\eta, \nabla \eta) \, \mathrm{d}X, \qquad F_{\mathrm{int}} = \gamma \left(\frac{3\ell}{2} |\nabla \eta|^2 + \frac{6}{\ell} \eta^2 (1-\eta)^2 \right). \tag{7}$$

Here, F_{int} denotes the interfacial energy density (per unit volume), ℓ is the interface thickness parameter, and γ is a material parameter characterizing the interfacial energy (per unit area), also called the surface tension. The first term inside the parentheses accounts for the gradient energy (assumed here isotropic), while the second (algebraic) term corresponds to the local bulk (or potential) energy contribution.

When generalized to $N+1$ phases, the interfacial energy density (7) is considered in the following multiwell form:

$$F_{\mathrm{int}} = \sum_{i=0}^{N} \left(\kappa_i |\nabla \eta_i|^2 + \varepsilon_i \eta_i^2 (1-\eta_i)^2 \right) = \nabla \boldsymbol{\eta} \cdot \mathbb{H} \nabla \boldsymbol{\eta} + F_{\mathrm{int}}^{\mathrm{alg}}(\boldsymbol{\eta}), \tag{8}$$

where $\mathbb{H}$ is the *capillary matrix*, $\mathbb{H} = \mathrm{diag}(\kappa_0, \dots, \kappa_N)$, and $F_{\mathrm{int}}^{\mathrm{alg}}$ denotes the algebraic part of the interfacial energy, $F_{\mathrm{int}}^{\mathrm{alg}} = \sum_{i=0}^{N} \varepsilon_i \eta_i^2 (1-\eta_i)^2$. The symbol $\cdot$ represents the full contraction of two tensors resulting in a scalar.[1] The above form of the interfacial energy, although not the most general (as it represents a diagonal closure), possesses several desirable properties. Most notably, it reduces transparently to the standard two-phase formulation for any purely two-phase state. We refer to this property as:

Algebraic Consistency (AC). (also referred to as the "P1" condition by Boyer and Lapuerta (2006)): *The interfacial energy function $F_{\mathrm{int}}(\boldsymbol{\eta}, \nabla \boldsymbol{\eta})$ reduces to the two-phase expression (7) for any composition vector of the form*

$$\boldsymbol{\eta} = \eta_i \mathbf{e}_i + (1-\eta_i)\mathbf{e}_j, \quad \nabla \boldsymbol{\eta} = \nabla \eta_i (\mathbf{e}_i - \mathbf{e}_j), \qquad 0 \le i \ne j \le N, \quad \eta_i \in (0,1),$$

with appropriately chosen parameters ℓ and γ.

This property allows the parameters κ_i and ε_i to be directly interpreted in terms of the physical surface tensions γ_{ij} and diffuse interface thicknesses ℓ_{ij} between phase pairs i and j.[2]

[1] Two matrices $\nabla \boldsymbol{\alpha}, \nabla \boldsymbol{\beta}$ are contracted in the following way

$$\nabla \boldsymbol{\alpha} \cdot \nabla \boldsymbol{\beta} = \sum_{j=1}^{d} \sum_{i=0}^{N} \frac{\partial \alpha_i}{\partial x_j} \frac{\partial \beta_i}{\partial x_j}, \quad \text{i.e.} \quad \nabla \boldsymbol{\eta} \cdot \mathbb{H} \nabla \boldsymbol{\eta} = \sum_{k=1}^{d} \sum_{m=0}^{N} \sum_{n=0}^{N} \mathbb{H}_{mn} \frac{\partial \eta_m}{\partial x_k} \frac{\partial \eta_n}{\partial x_k}.$$

In line with the specific application under consideration, we further assume that *only two types of interfaces are present in our system*: β–ω_i interfaces and ω_i–ω_j interfaces, characterized by the surface tensions $\gamma_{\beta\omega}$ and $\gamma_{\omega\omega}$, and corresponding interface thicknesses $\ell_{\beta\omega}$ and $\ell_{\omega\omega}$, respectively. As discussed in the Introduction, the direct ω_i–ω_j interfaces are in fact not allowed, and the model will be modified to meet this requirement.

3.1.1. Identification of κ_i and ε_i

We now provide an explicit identification of the parameters κ_i and ε_i in terms of interfacial surface tensions and diffuse interface thicknesses. This is done by inspecting the expression (8) for purely two-phase states (for each pairwise interaction), and comparing it with the standard two-phase form (7).

For clarity, we first illustrate the procedure in the three-phase case (i.e., $N = 2$ in Eq. (8)):

- Consider a mixed two-phase state involving β and ω_1. Set $\eta_2 = 0$ and define $\eta_0 = 1 - \eta_1$. Substituting into (8) yields:

$$F_{\text{int}} = (\kappa_0 + \kappa_1)|\nabla\eta_1|^2 + (\varepsilon_0 + \varepsilon_1)\eta_1^2(1-\eta_1)^2.$$

  By comparing with the standard two-phase form:

$$F_{\text{int}} = \gamma_{\beta\omega}\left(\frac{3\ell_{\beta\omega}}{2}|\nabla\eta_1|^2 + \frac{6}{\ell_{\beta\omega}}\eta_1^2(1-\eta_1)^2\right), \tag{9}$$

  we obtain the relations:

$$\kappa_0 + \kappa_1 = \frac{3\gamma_{\beta\omega}\ell_{\beta\omega}}{2}, \quad \varepsilon_0 + \varepsilon_1 = \frac{6\gamma_{\beta\omega}}{\ell_{\beta\omega}}.$$

- Similarly, for a β–ω_2 mixture, setting $\eta_1 = 0$ and $\eta_0 = 1 - \eta_2$ gives:

$$\kappa_0 + \kappa_2 = \frac{3\gamma_{\beta\omega}\ell_{\beta\omega}}{2}, \quad \varepsilon_0 + \varepsilon_2 = \frac{6\gamma_{\beta\omega}}{\ell_{\beta\omega}}.$$

- For the ω_1–ω_2 interface, we fix $\eta_0 = 0$ and define $\eta_2 = 1 - \eta_1$, which yields:

$$\kappa_1 + \kappa_2 = \frac{3\gamma_{\omega\omega}\ell_{\omega\omega}}{2}, \quad \varepsilon_1 + \varepsilon_2 = \frac{6\gamma_{\omega\omega}}{\ell_{\omega\omega}}.$$

This results in a linear system of six equations in six unknowns (κ_0, κ_1, κ_2, ε_0, ε_1, ε_2) with a unique solution. This procedure generalizes straightforwardly to the case of $N + 1$ phases (β, ω_1, …, ω_N), and under the same modeling assumptions yields the unique solution:

$$\kappa_\beta = \kappa_0 = \frac{3}{4}(2\ell_{\beta\omega}\gamma_{\beta\omega} - \ell_{\omega\omega}\gamma_{\omega\omega}), \quad \kappa_\omega = \kappa_1 = \cdots = \kappa_N = \frac{3}{4}\ell_{\omega\omega}\gamma_{\omega\omega}, \tag{10}$$

$$\varepsilon_\beta = \varepsilon_0 = 3\left(\frac{2\gamma_{\beta\omega}}{\ell_{\beta\omega}} - \frac{\gamma_{\omega\omega}}{\ell_{\omega\omega}}\right), \quad \varepsilon_\omega = \varepsilon_1 = \cdots = \varepsilon_N = 3\frac{\gamma_{\omega\omega}}{\ell_{\omega\omega}}, \tag{11}$$

with a new notation (κ_β, κ_ω, ε_β, ε_ω) introduced for the parameters κ_i and ε_i.

3.2. Dissipation potential

We consider a particularly simple form of the dissipation potential, given in a diagonal form:

$$D = \int_\Omega D(\dot{\boldsymbol{\eta}})\,\mathrm{d}X, \qquad D = \sum_{i=0}^{N}\frac{\dot{\eta}_i^2}{2m_i} = \frac{1}{2}\dot{\boldsymbol{\eta}}\cdot\mathbb{M}\,\dot{\boldsymbol{\eta}}, \tag{12}$$

where $m_i > 0$ denotes the mobility parameter associated with phase i, and $\mathbb{M}$ is the *mobility matrix*, $\mathbb{M} = \mathrm{diag}(1/m_0, \ldots, 1/m_N)$. Referring to the special case considered here – with N equivalent ω variants – effectively there are two, possibly distinct mobility parameters m_β and m_ω, such that $m_0 = m_\beta$ and $m_i = m_\omega$ for $i = 1, \ldots, N$.

As with the gradient part of the energy functional, it is shown in Appendix A that, upon enforcing the sum-to-unity constraint $(1)_3$, the general form of the dissipation potential with non-diagonal terms in the mobility matrix $\mathbb{M}$ is *equivalent* to the simple diagonal form in Eq. (12).

---

[2] We note that, for a more general ansatz

$$F_{\text{int}} = \sum_{0\le i<j\le N}\left(\kappa_{ij}\nabla\eta_i\cdot\nabla\eta_j + \varepsilon_{ij}\eta_i^2\eta_j^2\right),$$

which includes off-diagonal terms both in the algebraic and gradient parts of energy, it is shown in Appendix A that, in the setting of our model, the gradient part is, in fact, equivalent to the chosen diagonal form. On the other hand, the off-diagonal form of the algebraic part of the energy was rejected by Boyer and Lapuerta (2006) as being incompatible with the assumptions of algebraic and dynamic (evolutionary) consistency.

3.3. Ensuring the sum-to-unity constraint: reduced dissipation and energy functionals

Having defined the energy functional (8) and the dissipation potential (12), we must ensure that the constraint $\sum_{i=0}^{N}\eta_i = 1$, see Eq. $(1)_3$, is preserved by the evolution Eq. (3). There are at least two standard approaches to enforce this condition. The first is to *directly use the constraint to eliminate one of the η_i variables*. The second is to impose the constraint using a *Lagrange multiplier method*. In this work, we adopt the former approach; however, it can be shown that the alternative method using a Lagrange multiplier leads to an equivalent evolution. The main advantage of the elimination method is a reduction in the number of variables. Its primary drawback is the loss of the diagonal structure of the dissipation and energy functionals.

By expressing the order parameter of phase 0 via the sum-to-unity constraint as $\eta_0 = 1 - \sum_{i=1}^{N}\eta_i$, and substituting this into the energy and dissipation functionals (8) and (12), we obtain the following *reduced-form* expressions:

$$\hat{D}(\dot{\hat{\boldsymbol{\eta}}}) = \frac{1}{2}\dot{\hat{\boldsymbol{\eta}}}\cdot\hat{\mathbb{M}}\,\dot{\hat{\boldsymbol{\eta}}}, \qquad \hat{F}_{\mathrm{int}}(\hat{\boldsymbol{\eta}},\nabla\hat{\boldsymbol{\eta}}) = \nabla\hat{\boldsymbol{\eta}}\cdot\hat{\mathbb{H}}\,\nabla\hat{\boldsymbol{\eta}} + \hat{F}^{\mathrm{alg}}_{\mathrm{int}}(\hat{\boldsymbol{\eta}}), \tag{13}$$

where we have introduced the reduced (condensed) vector of order parameters, $\hat{\boldsymbol{\eta}}$, along with the corresponding auxiliary vectors $\hat{\mathbf{1}}$ and $\hat{\mathbf{e}}_i$, now of the length N, cf. Eq. (2),

$$\hat{\boldsymbol{\eta}} = (\eta_1,\dots,\eta_N)^{\mathrm{T}}, \qquad \hat{\mathbf{1}} = (1,\dots,1)^{\mathrm{T}}, \qquad \hat{\mathbf{e}}_i = (0,\dots,0,1,0,\dots,0)^{\mathrm{T}}. \tag{14}$$

The reduced mobility and capillary matrices have the following form,

$$\hat{\mathbb{M}} = m_\omega^{-1}\hat{\mathbb{I}} + m_\beta^{-1}\,\hat{\mathbf{1}}\otimes\hat{\mathbf{1}}, \qquad \hat{\mathbb{H}} = \kappa_\omega\hat{\mathbb{I}} + \kappa_\beta\hat{\mathbf{1}}\otimes\hat{\mathbf{1}}, \tag{15}$$

where $\hat{\mathbb{I}} = \mathrm{diag}(\hat{\mathbf{1}})$ is a $N\times N$ unit matrix, and $\hat{\mathbf{1}}\otimes\hat{\mathbf{1}}$ is a $N\times N$ matrix with all components equal to one. The reduced form of the algebraic part of the interfacial energy, $\hat{F}^{\mathrm{alg}}_{\mathrm{int}}$, is obtained simply by substituting $\boldsymbol{\eta} = \boldsymbol{\eta}(\hat{\boldsymbol{\eta}})$ in the corresponding term in Eq. (8), thus $\hat{F}^{\mathrm{alg}}_{\mathrm{int}}(\hat{\boldsymbol{\eta}}) = F^{\mathrm{alg}}_{\mathrm{int}}(\boldsymbol{\eta}(\hat{\boldsymbol{\eta}}))$.

The evolution of $\hat{\boldsymbol{\eta}}$ is governed by the reduced evolution equation:

$$\frac{\delta\hat{D}(\dot{\hat{\boldsymbol{\eta}}})}{\delta\dot{\hat{\boldsymbol{\eta}}}} + \frac{\delta\hat{F}(\hat{\boldsymbol{\eta}})}{\delta\hat{\boldsymbol{\eta}}} = \mathbf{0}, \tag{16}$$

where the reduced functionals $\hat{F}$ and $\hat{D}$ are the volume integrals of the local potentials $\hat{F}$ and $\hat{D}$, in analogy to Eqs. (7) and (12).

3.4. Structural requirements on the energy and dissipation functionals

We now impose the structural constraints that the reduced functionals $\hat{D}$ and $\hat{F}$ must satisfy. Specifically, we assert the following:

- The reduced dissipation matrix $\hat{\mathbb{M}}$ must be *positive semidefinite* in order to comply with the second law of thermodynamics. Indeed, the dissipation rate ξ on the manifold $\sum_{i=0}^{N}\eta_i = 1$ is given by

$$\xi = \sum_{i=1}^{N}\frac{\partial\hat{D}}{\partial\dot{\eta}_i}\dot{\eta}_i = \dot{\hat{\boldsymbol{\eta}}}\cdot\hat{\mathbb{M}}\,\dot{\hat{\boldsymbol{\eta}}},$$

  so the non-negativity of ξ for arbitrary processes, as required by the second law, is equivalent to the positive semidefiniteness of $\hat{\mathbb{M}}$.[3]
- Similarly, the capillary matrix $\hat{\mathbb{H}}$ must be *positive definite*. Negative eigenvalues would allow the total energy to decrease indefinitely through appropriately tailored interfaces, a scenario that is not physically admissible. Zero eigenvalues would imply that certain gradient directions contribute no energy, so variations along those directions would not be penalized. This would prevent control over the interface structure. Positive definiteness ensures that the energy is bounded from below and that all gradient contributions are properly controlled, see also (Boyer & Lapuerta, 2006). This condition is further discussed later.

3.5. Governing equations

The reduced Ginzburg–Landau evolution equation (16) can now be recast in the following form

$$\hat{\mathbb{M}}\,\dot{\hat{\boldsymbol{\eta}}} = \hat{\mathbb{H}}\,\Delta\hat{\boldsymbol{\eta}} + \hat{\mathbf{f}}(\hat{\boldsymbol{\eta}}), \qquad \hat{\mathbf{f}}(\hat{\boldsymbol{\eta}}) = -\frac{\partial\hat{F}}{\partial\hat{\boldsymbol{\eta}}} = \hat{\mathbf{f}}_{\mathrm{chem}}(\hat{\boldsymbol{\eta}}) + \hat{\mathbf{f}}_{\mathrm{int}}(\hat{\boldsymbol{\eta}}), \tag{17}$$

where Δ denotes the Laplacian operator, the chemical driving force $\hat{\mathbf{f}}_{\mathrm{chem}} = -\partial\hat{F}_{\mathrm{chem}}/\partial\hat{\boldsymbol{\eta}}$ is now left unspecified, and the driving force corresponding to the algebraic part of the double-well interfacial energy (8) reads

$$\hat{\mathbf{f}}_{\mathrm{int}}(\hat{\boldsymbol{\eta}}) = -\frac{\partial\hat{F}^{\mathrm{alg}}_{\mathrm{int}}}{\partial\hat{\boldsymbol{\eta}}} = 2\varepsilon_\beta\eta_0(1-\eta_0)(1-2\eta_0)\Big|_{\eta_0=1-\sum_{i=1}^{N}\eta_i}\hat{\mathbf{1}} - \sum_{i=1}^{N}2\varepsilon_\omega\eta_i(1-\eta_i)(1-2\eta_i)\hat{\mathbf{e}}_i. \tag{18}$$

[3] This is guaranteed for $m_\omega > 0$ and $m_\beta > 0$, but also for a somewhat non-intuitive case of $m_\omega > 0$ and $m_\beta \le -N m_\omega$.

Multiplying Eq. (17) by $\hat{\mathbb{M}}^{-1}$ from the left yields

$$\dot{\hat{\boldsymbol{\eta}}} = \hat{\mathbb{M}}^{-1}\hat{\mathbb{H}}\,\Delta\hat{\boldsymbol{\eta}} + \hat{\mathbb{M}}^{-1}\hat{\mathbf{f}}(\hat{\boldsymbol{\eta}}), \tag{19}$$

a preferable and insightful form of the evolutionary system that allows us to impose an additional important requirement on our model, the *evolutionary consistency* of two-phase states.

4. Requirement of evolutionary consistency of the two-phase states

In this section, we first consider a special case when the chemical driving force vanishes, $\hat{\mathbf{f}}_{\text{chem}} = \mathbf{0}$, so that $\hat{\mathbf{f}} = \hat{\mathbf{f}}_{\text{int}}$. Accordingly, the evolution is driven solely by the interfacial energy. As the next step, the chemical driving force is considered in Section 5.

In addition to the AC requirement (consistency with two-phase systems), it is natural to impose its dynamic counterpart—referred to as the "P2" requirement by Boyer and Lapuerta (2006). Specifically, it is reasonable to assume that if a certain phase is absent initially, it should not spontaneously appear in the absence of external thermal, mechanical, or chemical forcing.

In the context of multi-phase systems, this leads to a complex set of constraints. Therefore, for the purposes of this study, we adopt a simplified (weaker) version of this assumption, formulated specifically for arbitrary two-phase mixed states:

Evolutionary Consistency (EC). *If the multi-phase system reduces (locally) to a purely two-phase mixed state, none of the absent phases should emerge spontaneously, i.e., without additional thermodynamic driving.*

This requirement pertains strictly to the interfacial contribution of the free energy; the "absence of external forcing" refers to the absence of energetic preference for specific phases by the bulk part of the energy. It is important to note that this dynamical condition thus does not apply under *arbitrary* thermodynamic forcing. For instance, elastic interactions may introduce an additional driving force if the stress fields of a newly nucleated variant partially compensate existing ones. In such cases, EC may no longer hold, and an initially two-phase system may evolve into a more complex multi-phase configuration.

On the other hand, in the context of our β–ω system, as the ω variants are chemically equivalent, the persistence of EC under purely chemical forcing will guide us in constructing a suitable chemical mixing term in Section 7.

4.1. Characterization and implications of the EC condition

Let us provide an explicit characterization of the EC condition in the setting of our model. The evolution equations for the reduced set of phase variables are given by Eq. (19). To evaluate whether the EC condition is satisfied, we first consider the two-component β–ω states, i.e., the case where $\eta_k \neq 0$, $\eta_0 = 1 - \eta_k$, while all other variants of ω are set to zero, i.e., $\hat{\boldsymbol{\eta}} = \eta_k\hat{\mathbf{e}}_k$. The EC condition is satisfied if only the kth ω variant remains present and all other variants remain absent, i.e., if (see Eq. (19))

$$\Delta\eta_k\,\hat{\mathbb{M}}^{-1}\hat{\mathbb{H}}\,\hat{\mathbf{e}}_k + \hat{\mathbb{M}}^{-1}\hat{\mathbf{f}}_{\text{int}}(\eta_k\hat{\mathbf{e}}_k) \sim \hat{\mathbf{e}}_k, \qquad k = 1,\dots,N. \tag{20}$$

Recall that $\hat{\mathbf{f}} = \hat{\mathbf{f}}_{\text{int}}$. Since the first term involves spatial derivatives of the field η_k, while the other is purely algebraic, it must hold separately:

$$\hat{\mathbb{M}}^{-1}\hat{\mathbb{H}}\,\hat{\mathbf{e}}_k \sim \hat{\mathbf{e}}_k, \tag{21}$$

$$\hat{\mathbb{M}}^{-1}\hat{\mathbf{f}}_{\text{int}}(\eta_k\hat{\mathbf{e}}_k) \sim \hat{\mathbf{e}}_k, \tag{22}$$

for $k = 1,\dots,N$. Alternatively, for the two-component ω–ω states, i.e., for composition vector $\hat{\boldsymbol{\eta}} = \eta_k\hat{\mathbf{e}}_k + (1-\eta_k)\hat{\mathbf{e}}_l$ $(l \neq k)$, the EC condition asserts that

$$\Delta\eta_k\,\hat{\mathbb{M}}^{-1}\hat{\mathbb{H}}\,(\hat{\mathbf{e}}_k - \hat{\mathbf{e}}_l) + \hat{\mathbb{M}}^{-1}\hat{\mathbf{f}}_{\text{int}}\left(\eta_k\hat{\mathbf{e}}_k + (1-\eta_k)\hat{\mathbf{e}}_l\right) \sim \hat{\mathbf{e}}_k - \hat{\mathbf{e}}_l, \qquad k,l = 1,\dots,N \;\; (k \neq l)\,. \tag{23}$$

As in the previous case, this implies two conditions:

$$\hat{\mathbb{M}}^{-1}\hat{\mathbb{H}}\,(\hat{\mathbf{e}}_k - \hat{\mathbf{e}}_l) \sim \hat{\mathbf{e}}_k - \hat{\mathbf{e}}_l, \tag{24}$$

$$\hat{\mathbb{M}}^{-1}\hat{\mathbf{f}}_{\text{int}}(\eta_k\hat{\mathbf{e}}_k + (1-\eta_k)\hat{\mathbf{e}}_l) \sim \hat{\mathbf{e}}_k - \hat{\mathbf{e}}_l. \tag{25}$$

While condition (24) follows from condition (21), the second condition (25) must be verified separately. Let us now inspect in detail the implications of all these requirements.

4.2. EC implication for the choice of mobilities

The first condition (21) implies that

$$\hat{\mathbb{H}} = \operatorname{diag}(M_\kappa^1,\dots,M_\kappa^N)\,\hat{\mathbb{M}}. \tag{26}$$

The special structure of $\hat{\mathbb{H}}$ and $\hat{\mathbb{M}}$ given in Eq. (15) moreover implies that all M_κ^i must be equal. Consequently, consistency with two-phase systems requires the relation

$$\hat{\mathbb{H}} = M_\kappa\hat{\mathbb{M}}, \tag{27}$$

for some positive (to ensure positive definiteness) scalar M_κ. This is a surprising requirement because it states that the matrix of mobilities $\hat{\mathbb{M}}$, characterizing the dissipation potential, must be linked to the matrix of energetic capillary coefficients $\hat{\mathbb{H}}$. Let us note that exactly this requirement has been introduced by Boyer and Lapuerta (2006) as a special choice of mobilities that allows enforcement of the sum-to-unity constraint in a three-phase Cahn–Hilliard model via a purely algebraic Lagrange multiplier.

This is not physically justifiable in general, however, in our specific setting, Eq. (27) is equivalent to (see Eq. (15))

$$m_\beta = M_\kappa \kappa_\beta^{-1} , \qquad m_\omega = M_\kappa \kappa_\omega^{-1} , \tag{28}$$

and we argue in the Discussion Section 9 that such a condition is not restrictive as it leaves enough freedom for an arbitrary choice of the so-called effective mobility of the β–ω interfaces.

4.3. EC implications for the energy coefficients

Let us inspect the second condition (22). We need an explicit expression for the inverse matrix $\hat{\mathbb{M}}^{-1} = M_\kappa \hat{\mathbb{H}}^{-1}$. As the matrix $\hat{\mathbb{H}}$ is a rank-one perturbation of a diagonal matrix, it can be easily inverted using the Sherman–Morrison formula as follows

$$\hat{\mathbb{H}}^{-1} = \frac{1}{\kappa_\omega}\hat{\mathbb{I}} - \frac{1}{\kappa_\omega(N + \kappa_\omega/\kappa_\beta)}\hat{\mathbf{1}} \otimes \hat{\mathbf{1}}. \tag{29}$$

Since

$$\hat{\mathbf{f}}(\eta_k \hat{\mathbf{e}}_k) = -2\eta_k(1-\eta_k)(1-2\eta_k)\left(\varepsilon_\beta \hat{\mathbf{1}} + \varepsilon_\omega \hat{\mathbf{e}}_k\right), \tag{30}$$

it suffices to evaluate

$$\hat{\mathbb{M}}^{-1}\left(\varepsilon_\beta \hat{\mathbf{1}} + \varepsilon_\omega \hat{\mathbf{e}}_k\right) = M_\kappa \frac{\varepsilon_\omega}{\kappa_\omega}\hat{\mathbf{e}}_k + \frac{M_\kappa}{N + \kappa_\omega/\kappa_\beta}\left(\frac{\varepsilon_\beta}{\kappa_\beta} - \frac{\varepsilon_\omega}{\kappa_\omega}\right)\hat{\mathbf{1}}. \tag{31}$$

In order for the last term to be proportional to $\hat{\mathbf{e}}_k$ as desired, and for this condition to be satisfied for an arbitrary β–ω_k pair, it must hold

$$\frac{\varepsilon_\beta}{\kappa_\beta} - \frac{\varepsilon_\omega}{\kappa_\omega} = 0. \tag{32}$$

Upon using relations between ε_i, κ_i and $\ell_{\beta\omega}, \ell_{\omega\omega}, \gamma_{\beta\omega}, \gamma_{\omega\omega}$, Eq. (11), we get that the EC condition for the β–ω states is satisfied only if the thickness parameters are the same, i.e.,

$$\ell_{\beta\omega} = \ell_{\omega\omega}. \tag{33}$$

This requirement of equality of interfacial thicknesses is another unexpected implication of the evolutionary consistency condition, and its consequences are investigated in the following section.

Before doing so, let us verify that condition (25) for the two-component ω–ω states is satisfied for the considered energy functional (8). Since it holds

$$\hat{\mathbf{f}}(\eta_k \hat{\mathbf{e}}_k + (1-\eta_k)\hat{\mathbf{e}}_l) = -2\varepsilon_\omega \eta_k(1-\eta_k)(1-2\eta_k)(\hat{\mathbf{e}}_k - \hat{\mathbf{e}}_l), \tag{34}$$

it suffices to observe that

$$\hat{\mathbb{M}}^{-1}\left(\hat{\mathbf{e}}_k - \hat{\mathbf{e}}_l\right) = M_\kappa \kappa_\omega^{-1}(\hat{\mathbf{e}}_k - \hat{\mathbf{e}}_l) , \tag{35}$$

implying that Eq. (25) holds.

4.4. Implication: inequality constraint on interfacial energies

The requirement of equality of interfacial thicknesses (33) translates via the assumption of positive definiteness of the reduced capillary matrix $\hat{\mathbb{H}}$ into a certain algebraic inequality constraint on the values of interfacial energies. In particular, it is demonstrated in Appendix B, that matrix $\hat{\mathbb{H}}$ given by Eq. $(15)_2$, with κ_β and κ_ω satisfying Eq. (10) is positive definite if and only if the following relation between the interfacial energies holds

$$\gamma_{\omega\omega} < \frac{2N}{N-1}\gamma_{\beta\omega}. \tag{36}$$

For $N = 2$, this condition yields $\gamma_{\omega\omega} < 4\gamma_{\beta\omega}$, equivalent in our setting to the condition articulated by Boyer and Lapuerta (2006) (Eq. (11) therein). For $N = 4$ (the case of our primary interest), condition (36) gives $\gamma_{\omega\omega} < \frac{8}{3}\gamma_{\beta\omega}$. This implies that the interfacial energy between two ω variants can be at most 8/3 times larger than the interfacial energy between the β phase and a single variant of ω. For further details, see Appendix B.

The consequences of the above inequalities are serious in cases when either physical setting or numerical reasoning requires to strongly penalize energetically the emergence of ω–ω interfaces, i.e., in cases, when it is desirable to make $\gamma_{\omega\omega}$ very large compared to $\gamma_{\beta\omega}$ energies. From a physical point of view, this situation is relevant in the so-called *total spreading* situation, when one of the coefficients κ_i in Eq. (8), see also Eq. (10), is negative (in our particular case, this concerns $\kappa_0 = \kappa_\beta$, see Section 6).

5. Chemical energy

Up to this point, the model has accounted solely for the interfacial energy. However, in many cases, including in titanium alloys exhibiting the parental phase β and four variants of the ω phase, phase stability is influenced by both temperature and the local concentration of molybdenum. Under appropriate conditions, certain phases may become energetically favorable, introducing a chemical driving force that promotes their formation. It is important to note that all four ω variants are chemically equivalent, and thus the chemical free energy does not distinguish between them.

Generally, the chemical energy of the system is given by

$$\mathcal{F}_{\text{chem}} = \int_{\Omega} F_{\text{chem}} \, \mathrm{d}X, \qquad F_{\text{chem}} = h_{\text{mix}} \Delta G, \tag{37}$$

where the chemical energy density F_{chem} is given by the Gibbs energy difference between the two pure phases $\Delta G = G_\omega - G_\beta$ and by a suitable mixing function h_{mix}, ensuring smooth interpolation between them. We assume here that ΔG is spatially homogeneous and constant in time, which is sufficient for the purpose of this work. In a more general setting, this assumption can be relaxed.

5.1. Two-phase system

In the case of two phases (one ω variant and the β phase), the system is described by a single order parameter η_1, with $\eta_0 = 1 - \eta_1$ due to the sum-to-unity constraint. The chemical mixing is modeled using a smooth interpolation function $\varphi(\eta_1)$, defined as (see (Wang et al., 1993)):

$$\varphi(\eta_1) = \begin{cases} 0 & \eta_1 < 0, \\ 3\eta_1^2 - 2\eta_1^3 & \eta_1 \in [0,1], \\ 1 & \eta_1 > 1, \end{cases} \tag{38}$$

This cubic polynomial satisfies $\varphi(0) = 0$ in the pure β phase and $\varphi(1) = 1$ in the pure ω phase, with zero derivatives at both ends. As a result, the chemical driving force vanishes in the pure phases, ensuring local equilibrium. The capping outside $[0,1]$ prevents unphysical energy contributions. Alternative interpolation functions with similar properties, such as $\varphi(\eta_1) = \eta_1^3(6\eta_1^2 - 15\eta_1 + 10)$, can also be used (Moelans et al., 2008).

Finally, the function is symmetric with respect to the two phases:

$$\varphi(\eta_1) = \varphi(1 - \eta_0) = 1 - \varphi(\eta_0), \tag{39}$$

reflecting their equivalent roles in the two-phase system. Thus, the chemical energy reads

$$F^{(2)}_{\text{chem}} = h^{(2)}_{\text{mix}} \Delta G, \qquad h^{(2)}_{\text{mix}} = \varphi(\eta_1), \tag{40}$$

with the superscript "(2)" indicating the two-phase system.

5.2. $(N+1)$-phase system

Although the chemical energy $F^{(2)}_{\text{chem}}$ was originally designed for two-phase systems, its structure can be naturally extended to model multi-variant systems consisting of a parent β phase and N chemically equivalent ω variants. In this setting, the order parameter η_0 represents the β phase, while $\eta_1, \dots, \eta_N$ describe the individual ω variants. All order parameters are subject to the standard sum-to-unity constraint.

Crucially, the ω variants are assumed to be chemically equivalent. Accordingly, the chemical energy should depend only on the total amount of the ω phase and not on the particular variant. This assumption must be reflected in the structure of the mixing function, which treats all ω variants symmetrically.

Consider thus the chemical energy and the corresponding mixing function for the $(N+1)$-phase model in the following form,

$$F^{(N+1)}_{\text{chem}} = \Delta G \, h^{(N+1)}_{\text{mix}}, \qquad h^{(N+1)}_{\text{mix}} = 1 - \varphi(\eta_0). \tag{41}$$

This mixing function vanishes in the pure β phase ($\eta_0 = 1$) and equals one in any pure (or mixed) ω configuration ($\eta_0 = 0$). It does not distinguish between individual ω variants, which is appropriate given their chemical equivalence. It satisfies the algebraic consistency trivially, however, this formulation does *not* satisfy the evolutionary consistency (EC) condition, a point that will be discussed in detail in Section 7.

Before introducing a chemical energy that fulfills the EC condition, it is instructive to explore how the phase behavior changes when the chemical driving force becomes dominant. In particular, we investigate the competition between chemical and interfacial energies in the so-called *total spreading case*, where the system energetically favors separation of distinct ω variants by an intervening β phase. This regime highlights the limitations of standard mixing approaches and motivates the development of a more consistent formulation, especially when $\Delta G < 0$.

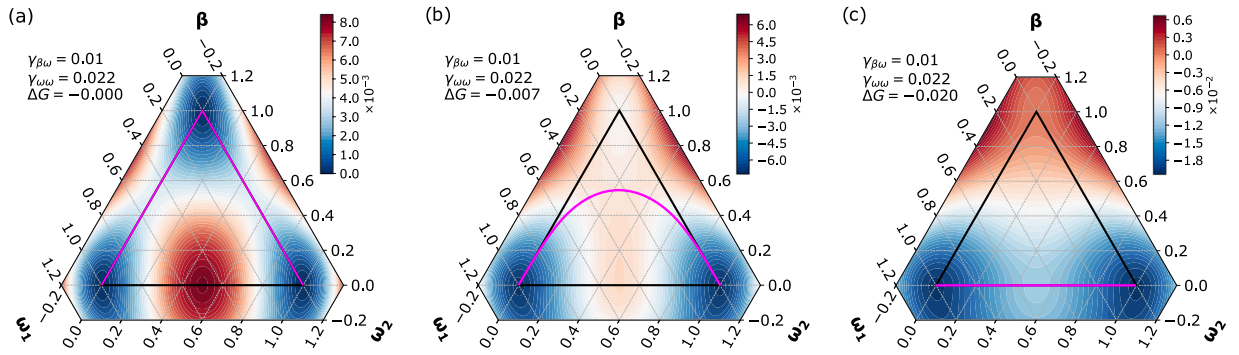

Fig. 1. The influence of chemical energy forcing on the multiwell potential in the reference total-spreading regime. The magenta lines indicate approximate *least-energy* paths between the two ω states. (a) For $\Delta G = 0$, the lowest-energy configuration is represented by the two-phase states ω_1–β and ω_2–β. (b) For $\Delta G = -0.007$ GPa, the energetically preferred path traverses the central region of the simplex, allowing for a mixed three-phase ω_1–β–ω_2 state. (c) For an even larger chemical driving force, $\Delta G = -0.02$ GPa, the nearly direct ω_1–ω_2 path becomes energetically favored, despite being non-physical. In all cases, the chemical energy (41) has been used. Here and henceforth, the units of $\gamma_{\beta\omega}$, $\gamma_{\omega\omega}$, ΔG are J/m^2, J/m^2, GPa, see (42).

6. Total spreading case

In this paper, we aim to develop a model capable of describing a material in which two different variants of the ω phase cannot coexist directly; they must always be separated by a β phase. This situation is commonly referred to as the *total-spreading case*. It arises when the interfacial energy between the β phase and any variant of ω is at least twice as small as the interfacial energy between two ω variants, making it energetically favorable to insert a β phase between them (i.e., to form two β–ω interfaces). However, this characterization of the total spreading case holds only in the absence of other driving forces, such as chemical ones.

In the following, we include the chemical contribution, focusing on the regime that favors the precipitation of ω phases, i.e., where the chemical energy difference $\Delta G = G_\omega - G_\beta$ is non-positive. Within this regime, we distinguish between the case where the chemical driving force is absent ($\Delta G = 0$) and the case where it is present ($\Delta G < 0$).

From now on, we employ ternary plots of the energy landscape (algebraic part of the free energy, here, corresponding to $N = 2$) to illustrate the key features of the model (Fig. 1). The top vertex of the triangle corresponds to the pure β phase, while the two lower corners represent the two variants of the ω phase. The physically admissible simplex ($\eta_i \in [0, 1]$) is outlined with a thick black line. Ternary plots are chosen for their simplicity—in the actual case of $N = 4$, the corresponding topology is a *5-cell*, a four-dimensional object that is difficult to visualize.

In the following illustrative examples, the material parameters ($\gamma_{\beta\omega}$, ΔG, $\ell_{\beta\omega}$) take realistic values for the β–ω transition in Ti alloys, as specified in Section 8. Units, if omitted, are

$$[\ell_{\beta\omega}] = [\ell_{\omega\omega}] = \text{nm}, \qquad [\Delta G] = [\lambda] = \text{nN/nm}^2 = \text{J/mm}^3 = \text{GPa}, \qquad [\gamma_{\beta\omega}] = [\gamma_{\omega\omega}] = \text{nN/nm} = \text{J/m}^2. \tag{42}$$

The case $\Delta G = 0$ (no chemical driving force) is shown in Fig. 1a, where total spreading is ensured by a sufficiently high energy barrier between ω_1 and ω_2 ($\gamma_{\omega\omega} > 2\gamma_{\beta\omega}$). In this case, the least-energy path in the energy landscape between the two ω variants avoids the ω–ω edge and instead passes through the β phase, as indicated by the magenta line. This suggests that the energetically favorable configuration begins in one of the ω variants, transitions through a mixed β–ω state into a pure β configuration, and then proceeds to form the other ω phase through a β–ω mixed state, eventually reaching the pure second variant of ω.

The least-energy paths serve as rough approximations – neglecting the gradient (capillary) contribution to the energy – of the composition profile (expressed in terms of the order parameters) across a hypothetical ω_1–ω_2 interface. In reality, the full transformation from ω_1 to β should occur first, followed by the conversion from β to ω_2. In the standard model, this behavior is observed only in the absence of chemical energy, $\Delta G = 0$, see Fig. 1a.

When a negative chemical energy difference is introduced (Fig. 1b), the energy of the two ω vertices decreases, and the least-energy path traverses a saddle point within the interior of the triangle. This point corresponds to a ternary state of ω_1–β–ω_2 coexistence, which we want to rule out as crystallographically inadmissible.

For even lower values of ΔG (Fig. 1c), with the least-energy path becoming the ω–ω edge, a direct ω_1–ω_2 interface forms (physically inadmissible), as the chemical energy contribution outweighs the interfacial energy cost. Note that $\Delta G \approx -0.02$ GPa is a typical value for the β–ω transformation at room temperature (Yan & Olson, 2016).

Based on this insight, one can argue that the most natural way to enforce the total-spreading situation would be to sufficiently increase $\gamma_{\omega\omega}$ to counteract the possible chemical energy forcing. However, this eventually conflicts with the positive definiteness condition (36) and therefore is not an admissible strategy for strongly negative ΔG. To overcome this limitation, a different approach is proposed in the next section.

6.1. Double-ditch model

We propose a modification of the model that is capable of describing the total spreading case, by augmenting suitably the algebraic part of the free energy analogously to (Boyer & Lapuerta, 2006). In our case, the idea is to relax the EC condition in the following sense: we still require it to hold for β–ω mixed states (interfaces), but we relax – even explicitly violate – it for the ω–ω interfaces. Consequently, if an ω–ω mixed state is taken as an initial condition, the β phase will spontaneously appear, separating the ω variants. All this is achieved by augmenting the algebraic part of the energy functional with what we nickname a "double-ditch" term, in the following manner:

$$F^*_{\mathrm{int}} = \sum_{i=0}^{N} \left(\kappa_i |\nabla \eta_i|^2 + \varepsilon_i \eta_i^2 (1-\eta_i)^2\right) + \lambda \underbrace{\sum_{1\le i<j\le N} \eta_i^2 \eta_j^2}_{\text{double ditch}}. \tag{43}$$

Here, $\lambda > 0$ is a coefficient that determines the magnitude of the double-ditch augmentation.

Note that the double-ditch augmentation in Eq. (43) extends the original diagonal form of the algebraic part of the interfacial energy (8) with the off-diagonal terms (see Footnote 2), though added here in a selective manner, i.e., only for the ω–ω pairs $(i, j \ge 1)$.

The double-ditch term clearly does not affect the two-phase β–ω states, as it vanishes for these configurations. For all other states, it is positive and acts as an additional energetic barrier with maxima along the ω–ω interfaces, thereby shifting the energetic preference toward configurations that include an intermediate β phase.

Let us now investigate the impact of double-ditch augmentation of the energy functional on the fulfillment of the EC condition. Let us calculate an algebraic part of the thermodynamic driving force (see Eq. (17)) corresponding to energy (43)

$$\hat{\mathbf{f}}^*_{\mathrm{int}}(\hat{\boldsymbol{\eta}}) = -\frac{\partial \hat{F}^{*\mathrm{alg}}_{\mathrm{int}}}{\partial \hat{\boldsymbol{\eta}}} = \hat{\mathbf{f}}_{\mathrm{int}}(\hat{\boldsymbol{\eta}}) - 2\lambda \sum_{i=1}^{N} \eta_i \hat{\mathbf{e}}_i \left(\sum_{j=1, j\neq i}^{N} \eta_j^2 \right), \tag{44}$$

with $\hat{\mathbf{f}}_{\mathrm{int}}(\hat{\boldsymbol{\eta}})$ given by Eq. (18). Since the gradient part of the free energy is unaffected by the augmentation, EC conditions (21) and (24) remain satisfied. Concerning analogues of conditions (22) and (25), we obtain by direct calculation:

$$\hat{\mathbf{f}}^*(\eta_k \hat{\mathbf{e}}_k) = \hat{\mathbf{f}}(\eta_k \hat{\mathbf{e}}_k), \tag{45}$$

$$\hat{\mathbf{f}}^*(\eta_k \hat{\mathbf{e}}_k + (1-\eta_k)\hat{\mathbf{e}}_l) = \hat{\mathbf{f}}(\eta_k \hat{\mathbf{e}}_k + (1-\eta_k)\hat{\mathbf{e}}_l) - 2\lambda \eta_k (1-\eta_k)(\hat{\mathbf{e}}_k - \eta_k(\hat{\mathbf{e}}_k - \hat{\mathbf{e}}_l)). \tag{46}$$

Consequently, the EC condition for the β–ω states remains valid for the augmented energy functional, since (under the same conditions (33)) we get

$$\hat{\mathbb{M}}^{-1} \hat{\mathbf{f}}^*_{\mathrm{int}}(\eta_k \hat{\mathbf{e}}_k) \sim \hat{\mathbf{e}}_k. \tag{47}$$

But the EC condition for the ω–ω states becomes now violated since Eq. (46) implies

$$\hat{\mathbb{M}}^{-1} \hat{\mathbf{f}}^*_{\mathrm{int}}(\eta_k \hat{\mathbf{e}}_k + (1-\eta_k)\hat{\mathbf{e}}_l) \nsim \hat{\mathbf{e}}_k - \hat{\mathbf{e}}_l. \tag{48}$$

To summarize, the double-ditch augmentation of the energy functional satisfies the EC condition (or equivalently the "P2" condition as introduced by Boyer and Lapuerta (2006)) for the two-component β–ω states, but violates it for the two-component ω–ω states. While Boyer and Lapuerta (2006) rejected the off-diagonal (i.e., our double-ditch) terms in the algebraic part of the free energy, here, in the context of our target application, such a violation is a desirable feature since we require these unphysical ω–ω states to be unstable.

6.2. Interpretation of the double-ditch augmentation for a three-phase model

Let us now demonstrate the performance of the model with double-ditch augmentation and provide its deeper interpretation in the simplest, i.e., three-phase setting ($N = 2$). In this setting, the interfacial energy density is given by

$$F^*_{\mathrm{int}} = \sum_{i=0}^{2} \left(\kappa_i |\nabla \eta_i|^2 + \varepsilon_i \eta_i^2 (1-\eta_i)^2\right) + \lambda \eta_1^2 \eta_2^2, \tag{49}$$

where the double-ditch term $\lambda \eta_1^2 \eta_2^2$ penalizes the mixed ω_1–ω_2 states by introducing a potential barrier that reaches its maximum along the ω_1–ω_2 edge. This augmentation energetically favors configurations in which an interstitial β phase separates the adjacent ω variants, see Fig. 2.

Let us now document the main advantage of the double-ditch augmentation by showing that it enables us to effectively increase the interfacial energy between different ω variants arbitrarily. Importantly, since the augmentation is purely algebraic, it does not interfere with the (positive definiteness) condition of the capillary matrix given in Eq. (36). As we shall see, in this sense, the double-ditch term circumvents the intrinsic limitations of the standard model. The only (beneficial) trade-off is the loss of the EC condition for mixed ω–ω states.

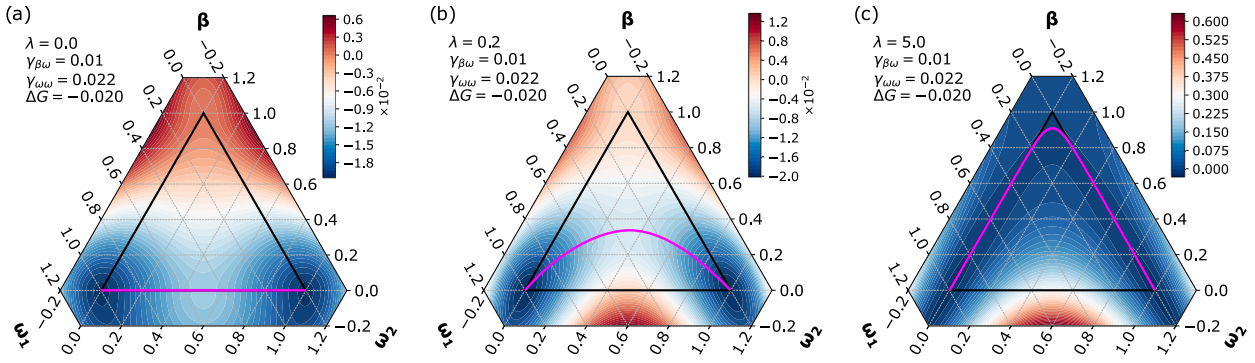

Fig. 2. The impact of the double-ditch augmentation on the multiwell potential with nonzero chemical energy for $N = 2$. The magenta lines indicate the approximate least-energy paths, as in Fig. 1. (a) In the reference model with $\lambda = 0$, a direct ω_1–ω_2 interface forms. (b) For $\lambda = 0.2$ GPa, the direct interface is penalized, and the path is pushed toward a ternary mixed state involving β. (c) For a stronger augmentation, $\lambda = 5$ GPa, the interface is forced to pass through a nearly pure β state.

So let us consider the augmented energy (49) in the ω_1–ω_2 mixed state (i.e., for $\eta_0 = 0$ and $\eta_2 = 1 - \eta_1$), and using the fact that $\kappa_\omega = \kappa_1 = \kappa_2$ and $\varepsilon_\omega = \varepsilon_1 = \varepsilon_2$ we get the corresponding two-phase energy in the form

$$F^*_{\text{int}} = 2\kappa_\omega |\nabla\eta_1|^2 + (2\varepsilon_\omega + \lambda)\eta_1^2(1-\eta_1)^2.$$

We can now interpret it in terms of effective surface tension $\gamma^{\text{eff}}_{\omega\omega}$ and effective interface thickness $\ell^{\text{eff}}_{\omega\omega}$ as follows. By comparing this result with the corresponding two-phase formula, see Eq. $(7)_1$,

$$F^*_{\text{int}} = \gamma^{\text{eff}}_{\omega\omega}\left(\frac{3\ell^{\text{eff}}_{\omega\omega}}{2}|\nabla\eta_1|^2 + \frac{6}{\ell^{\text{eff}}_{\omega\omega}}\eta_1^2(1-\eta_1)^2\right), \tag{50}$$

we obtain, after expressing the effective parameters, the following formulas

$$\gamma^{\text{eff}}_{\omega\omega} = \sqrt{\frac{2\kappa_\omega(2\varepsilon_\omega+\lambda)}{9}} = \gamma_{\omega\omega}\sqrt{1+\frac{\lambda}{2\varepsilon_\omega}}, \qquad \ell^{\text{eff}}_{\omega\omega} = \sqrt{\frac{8\kappa_\omega}{2\varepsilon_\omega+\lambda}} = \frac{\ell_{\omega\omega}}{\sqrt{1+\frac{\lambda}{2\varepsilon_\omega}}}. \tag{51}$$

These formulas provide the desired interpretation of the augmentation: by increasing the value of the parameter λ, we scale up the effective surface tension between the two ω phases, while simultaneously reducing the effective interface thickness between them. Crucially, this modification is introduced solely through the algebraic part of the interfacial free energy, meaning that the positive definiteness requirement of the capillary matrix, Eq. (36), remains unaffected.

Thus, starting with a choice of parameters κ_β and κ_ω such that the positive definiteness assumption on the capillary matrix holds, and then augmenting the free energy by the double-ditch term, we can arbitrarily exceed the limitations inherently present in the standard (EC) model for total spreading cases, as expressed in Eq. (36). Specifically, we can make the (effective) interfacial energy between the selected ω variants arbitrarily large. Through this mechanism, our model effectively prevents the formation of mixed ω–ω states, since an appropriately chosen value of λ penalizes such configurations to any desired degree. Importantly, this augmentation leaves the energy of physically admissible mixed β–ω states unchanged and it does not violate the EC condition for these states, as the term and its partial derivatives are zero-valued here.

To summarize: *By augmenting the interfacial energy with double-ditch terms using a sufficiently large λ, we effectively eliminate the existence of mixed ω–ω states under arbitrary chemical forcing, without affecting the physically admissible β–ω configurations or compromising their EC stability.*

7. Evolutionary consistent chemical mixing

In our particular application, all the variants of the ω phase are chemically equivalent. It is thus natural to extend the EC condition for the physically relevant β–ω states also to the chemical part of the bulk free energy. To motivate this extension, consider a ternary system ($N = 2$) and a configuration in which only β and ω_1 are present and the chemical energy promotes further precipitation of the ω phase. Since all ω variants are chemically equivalent, no particular variant is energetically favored. Thus, precipitation of ω_1 reduces the chemical energy just as effectively as ω_2. However, the appearance of ω_2 introduces an interfacial interaction with ω_1, contributing additional (non-negative) interfacial energy. This penalty would not occur if more ω_1 formed instead. Consequently, the combined interfacial and chemical energy functional must reflect this assumption to enforce this behavior.

Thus, in addition to the EC condition for the interfacial energy (22), we impose an analogous condition on the chemical energy density $\hat{F}_{\text{chem}}$. In particular, we shall assert that (in an analogy with Eq. (30)) the chemical energy satisfies

$$\frac{\partial\hat{F}_{\text{chem}}}{\partial\hat{\boldsymbol{\eta}}}(\eta_k\hat{\mathbf{e}}_k) = \Delta G\frac{\partial h_{\text{mix}}}{\partial\hat{\boldsymbol{\eta}}}(\eta_k\hat{\mathbf{e}}_k) \sim \varepsilon_\beta\hat{\mathbf{1}} + \varepsilon_\omega\hat{\mathbf{e}}_k, \tag{52}$$

which ensures compliance with the EC condition of the total (interfacial + chemical) energy.

Notably, the simple mixing (41) violates this condition. Indeed, the corresponding driving force has the following form:

$$\hat{\mathbf{f}}_{\mathrm{chem}}^{(N+1)} = -\frac{\partial \hat{F}_{\mathrm{chem}}^{(N+1)}}{\partial \hat{\boldsymbol{\eta}}} = \Delta G\, \varphi'(\eta_0)\, \hat{\mathbf{1}}, \tag{53}$$

which is clearly incompatible with the form in Eq. (52) required for evolutionary consistency. In the following, we first document that this inconsistency can be mitigated by a sufficiently strong double-ditch augmentation. We then introduce a novel chemical mixing formulation – referred to as "elliptic mixing" – which inherently satisfies the required condition and overcomes the limitations of the simple model.

7.1. Simple mixing regularized by double-ditch potential

As shown above, the simple $(N+1)$-phase mixing function $h_{\mathrm{mix}}^{(N+1)}$ does not satisfy the EC condition. Specifically, the chemical driving force may point outward from the edge of the Gibbs simplex, leading the solution toward non-physical configurations in which multiple ω variants coexist (i.e., more than one $\eta_i > 0$). Since the double-ditch augmentation of the interfacial energy, introduced in Section 6.1, penalizes exactly the occurrence of such mixed states, it represents a natural candidate for regularization of the simple mixing model. Indeed, as documented in the numerical experiments in Section 8, by selecting a sufficiently large regularization parameter λ, the system is guided back toward physically meaningful configurations near the simplex edge with an accuracy sufficient in many practical situations.

The main drawback of this approach lies in the choice of λ: it is no longer directly tied to the physical interfacial energy $\gamma_{\omega\omega}^{\mathrm{eff}}$, but instead becomes a numerical tuning parameter dictated by simulation stability and accuracy. Furthermore, large values of λ may lead to slower convergence in numerical solvers.

7.2. Elliptic mixing

As a potential remedy to the EC inconsistency of the simple mixing model, we introduce one particular alternative formulation of chemical mixing that satisfies the EC condition, here referred to as *elliptic mixing*:

$$h_{\mathrm{mix}}^{\mathrm{elliptic}}(\hat{\boldsymbol{\eta}}) = \varphi(\eta_{\mathrm{eff}}), \qquad \eta_{\mathrm{eff}}(\hat{\boldsymbol{\eta}}) = \sqrt{\sum_{i=1}^{N} \eta_i^2 + 2\frac{\varepsilon_\beta}{\varepsilon_\beta + \varepsilon_\omega} \sum_{j>i\geq 1}^{N} \eta_i \eta_j}. \tag{54}$$

This mixing is called *elliptic*, since the function $\eta_{\mathrm{eff}} = \mathrm{const.}$ defines a surface of a rotational ellipsoid centered at $\eta_0 = 1$ and with the axis of rotation parallel to the $\eta_1 = \cdots = \eta_N$ line in the N-dimensional $\hat{\boldsymbol{\eta}}$ space. For $N = 2$, the function is plotted in Fig. 3a.

Compliance with the AC condition is trivial by a simple substitution $h_{\mathrm{mix}}^{\mathrm{elliptic}}(\eta_k \hat{\mathbf{e}}_k) = \varphi(\eta_{\mathrm{eff}}) = \varphi(\eta_k)$.

The EC compliance can be shown by taking the partial derivatives,

$$\frac{\partial h_{\mathrm{mix}}^{\mathrm{elliptic}}}{\partial \hat{\boldsymbol{\eta}}}(\hat{\boldsymbol{\eta}}) = \varphi'(\eta_{\mathrm{eff}}) \frac{\partial \eta_{\mathrm{eff}}}{\partial \hat{\boldsymbol{\eta}}}(\hat{\boldsymbol{\eta}}) = \frac{\varphi'(\eta_{\mathrm{eff}})}{\eta_{\mathrm{eff}}\left(\varepsilon_\beta + \varepsilon_\omega\right)} \left[\varepsilon_\beta \hat{\mathbf{1}} \sum_{i=1}^{N} \eta_i + \varepsilon_\omega \hat{\boldsymbol{\eta}}\right], \tag{55}$$

and substituting $\hat{\boldsymbol{\eta}} = \eta_k \hat{\mathbf{e}}_k$,

$$\frac{\partial h_{\mathrm{mix}}^{\mathrm{elliptic}}}{\partial \hat{\boldsymbol{\eta}}}(\eta_k \hat{\mathbf{e}}_k) = \frac{\varphi'(\eta_{\mathrm{eff}})}{\eta_{\mathrm{eff}}\left(\varepsilon_\beta + \varepsilon_\omega\right)} \left(\eta_k \varepsilon_\beta \hat{\mathbf{1}}_k + \eta_k \varepsilon_\omega \hat{\mathbf{e}}_k\right) \sim \varepsilon_\beta \hat{\mathbf{1}} + \varepsilon_\omega \hat{\mathbf{e}}_k, \tag{56}$$

which is the form derived in Eq. (30).

However, this function has an undesirable property, which can be immediately seen from the illustration in Fig. 3b. As the function $F_{\mathrm{chem}}^{\mathrm{elliptic}} = \varphi(\eta_{\mathrm{eff}})\Delta G$ is decreasing for $\Delta G < 0$ and $\eta_0 > 1$, non-physical minima may appear in conjunction with the multiwell potential in the $\eta_0 > 1$ region.

Therefore, we suggest adding a penalization h_{pen} as

$$h_{\mathrm{pen}} = \begin{cases} a\left(1-\eta_0\right)^2 \operatorname{sgn}(\Delta G) & \text{for } \eta_0 > 1, \\ 0 & \text{otherwise.} \end{cases} \tag{57}$$

It can be shown that $a > 3$ prevents the formation of minima, we used $a = 4$ to have a safe margin. Multiplying by $\operatorname{sgn}(\Delta G)$ is necessary to ensure that the penalization $h_{\mathrm{pen}}\Delta G$ is always positive. The elliptic chemical energy can therefore be written as

$$F_{\mathrm{chem}}^{\mathrm{elliptic}} = \left(h_{\mathrm{mix}}^{\mathrm{elliptic}} + h_{\mathrm{pen}}\right) \Delta G. \tag{58}$$

The proposed elliptic mixing satisfies the EC condition; however, it introduces a subtle inconsistency: the chemical energy is no longer constant for $\eta_0 = 0$ (at the ω-only subspace), and thus the expressions (51) for the interfacial parameters $\gamma_{\omega\omega}^{\mathrm{eff}}$ and $\ell_{\omega\omega}^{\mathrm{eff}}$ are no longer exactly valid. Nevertheless, this inconsistency leads to only a minor deviation in the interfacial energy. In all practical simulations, this approximation is acceptable and does not compromise the predictive power of the model. A more detailed numerical analysis is presented in Appendix C.

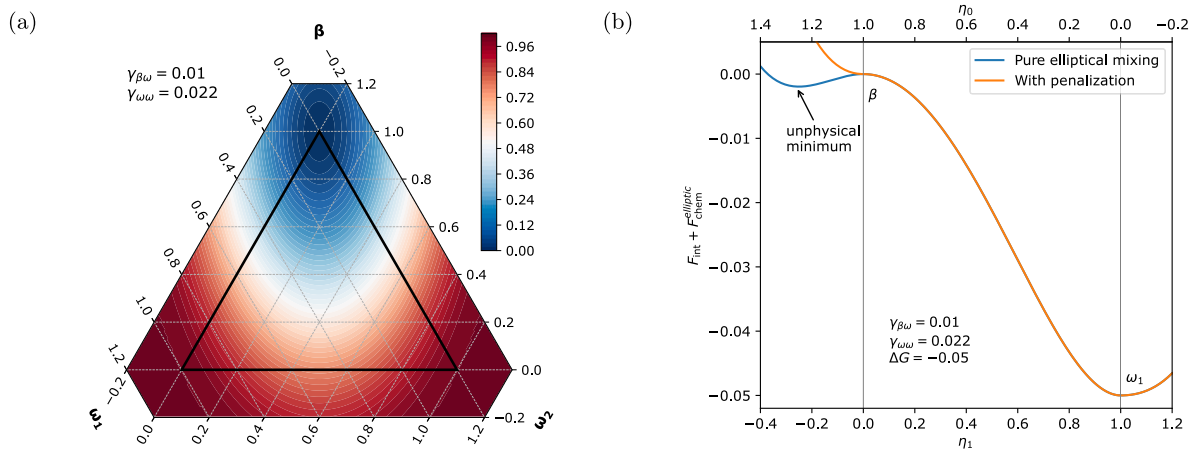

Fig. 3. Illustrations of the chemical energy mixing functions for two ω variants. (a) Elliptic mixing $h_{\text{mix}}^{\text{elliptic}}$ in ternary plot. (b) The free energy $F = F_{\text{int}} + F_{\text{chem}}^{\text{elliptic}}$ with and without the correction by h_{pen}: the profile of F along the β–ω_1 edge showing the presence of a non-physical minimum in the region $\eta_1 < 0$.

Furthermore, since the ω–ω interface is not observed experimentally, no direct data for $\gamma_{\omega\omega}$ are available. Our only modeling requirement is that the effective interfacial energy is sufficiently large to suppress the formation of such an interface, which is ensured by the double-ditch term. Therefore, minor deviations from $\gamma_{\omega\omega}^{\text{eff}}$ due to elliptical mixing do not affect the qualitative behavior of the model.

8. Numerical simulations

8.1. Finite-element implementation

The numerical implementation of the model is carried out using the Firedrake finite element library (Rathgeber et al., 2016). The computational domain is discretized uniformly: into line segments in 1D, quadrilaterals in 2D, and tetrahedra in 3D. The phase order parameters η_i are approximated using continuous, piecewise linear (1D), bi-linear (2D), or linear (3D) Lagrange elements.

Time integration is performed using the implicit backward Euler method, which ensures stability even for stiff problems. At each time step, the governing Eqs. (16) are obtained by computing variational derivatives of the total energy functional, which includes both the free energy F and the dissipation potential D. These derivatives are computed via automatic differentiation provided by Firedrake.

The resulting non-linear system is solved by Newton's method. To improve robustness, a line search strategy is employed, specifically the L2 line search implemented in the SNES interface of the PETSc library. The Jacobian matrix required in each Newton step is again obtained via automatic differentiation. The Newton solver uses strict convergence criteria, with relative and absolute tolerances set to 1×10^{-11} and 5×10^{-10}, respectively. The maximum number of Newton iterations per time step is limited to 12.

To control temporal resolution and computational cost, the time step size is adjusted adaptively. We monitor the number of Newton iterations required for convergence at each time step. If the number of iterations is below a target threshold (typically 7), the time step is increased; if it exceeds the threshold, the time step is reduced. The threshold values were determined empirically based on numerical experiments.

For solving the linear systems that arise within each Newton step, different strategies are applied depending on the spatial dimension. In 1D simulations, the system is small enough to permit the use of a direct solver (MUMPS). In 2D and 3D, iterative methods become necessary. As a preconditioner, we employ the BoomerAMG algebraic multigrid method from the Hypre package. The preconditioner uses classical interpolation, a standard technique in Ruge–Stüben AMG that constructs prolongation operators based on strong connections in the matrix. We use a maximum of 10 multigrid levels.

The multigrid preconditioner uses symmetric Gauss–Seidel method as the smoother for serial runs and Jacobi-based methods in parallel settings, both of which are the default options in BoomerAMG. This combination provides scalable and efficient performance for large and moderately ill-conditioned systems.

8.2. Specification of model parameters

Below, we present simulation results in one, two, and three spatial dimensions, all computed under a prescribed spatially homogeneous chemical driving force ΔG. Two distinct models for the chemical energy are employed: the simple mixing formulation (41), and the elliptic mixing model (58). The standard $(N+1)$-phase chemical energy model does not satisfy the EC condition, but it

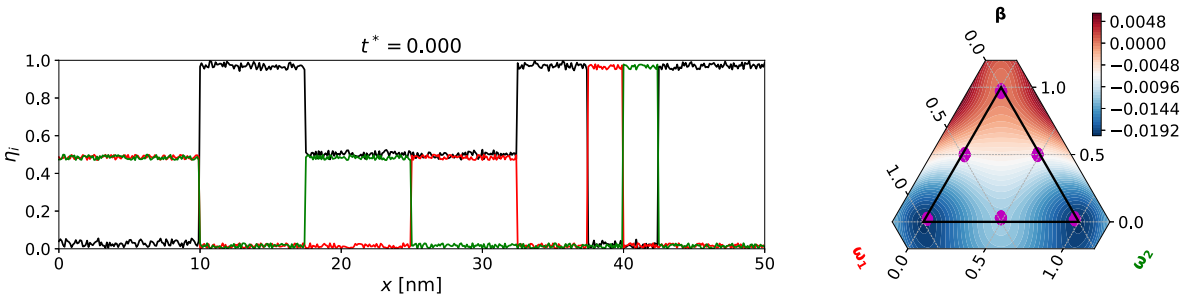

Fig. 4. Initial condition for the 1D numerical experiment ($N = 2$) illustrating the effect of chemical energy: the phase-field variables η_0 (black), η_1 (red), and η_2 (green) are plotted over the domain. The right panel displays the corresponding composition points in the ternary diagram (magenta bullets).

is straightforward to implement. In contrast, the elliptic mixing model satisfies the EC condition, although its implementation is somewhat more involved.

All simulations are computed for the following model parameters:

$$M_\kappa = 1\,\mathrm{nm}^2/\mathrm{s}, \qquad \gamma_{\beta\omega} = 0.01\,\mathrm{J/m}^2, \qquad \gamma_{\omega\omega} = 0.022\,\mathrm{J/m}^2, \qquad \ell_{\beta\omega} = \ell_{\omega\omega} = 1\,\mathrm{nm}, \qquad 0 \geq \Delta G \geq -0.02\,\mathrm{GPa}. \tag{59}$$

The above values of model parameters $\gamma_{\beta\omega}$, ΔG, and $\ell_{\beta\omega}$ are considered realistic for the β–ω transformation in Ti alloys, at least concerning the order of magnitude (Devaraj et al., 2012; Ehemann & Wilkins, 2017; Šmilauerová et al., 2017; Tang et al., 2012; Yan & Olson, 2016).

To satisfy the EC condition, the mobility parameters are adopted according to Eq. (27) so that $m_\beta = M_\kappa/\kappa_\beta$ and $m_\omega = M_\kappa/\kappa_\omega$. Parameter M_κ has been simply set equal to $1\,\mathrm{nm}^2/\mathrm{s}$ with no reference to a physically realistic time scale, thus specifying arbitrary units of time.

8.3. Ternary (N=2) 1D setting

We begin with one-dimensional numerical experiments for a ternary system composed of one parent β phase and two variants of the ω phase. The computational domain is the interval $[-25\,\mathrm{nm}, 25\,\mathrm{nm}]$, discretized using a uniform mesh with spacing $h = 0.1\,\mathrm{nm}$. Homogeneous Neumann boundary conditions are applied at both ends of the domain:

$$\frac{\partial \eta_i}{\partial x} = 0 \quad \text{at } x = \pm 25\,\mathrm{nm}. \tag{60}$$

This type of boundary condition does not impose any restriction with respect to the spatial dimension; periodic boundary conditions are used in higher-dimensional simulations to represent a domain surrounded by a similar material.

We structure this section as follows. First, we numerically demonstrate a key limitation of the standard model, namely its inability to achieve proper phase separation under sufficiently strong chemical driving. Next, we highlight the importance of the EC condition by violating the interfacial thickness equality constraint (33) and examining the consequences. Finally, we provide a comparative study of the two chemical mixing strategies – simple and elliptic – for various magnitudes of double-ditch regularization.

8.3.1. Lack of phase separation within the standard model

We first demonstrate that the standard double-well model fails to enforce separation of the ω variants by the β phase when the chemical driving force is sufficiently strong. The initial condition is shown in Fig. 4, and we use $\Delta G = -0.02\,\mathrm{GPa}$, $\gamma_{\beta\omega} = 0.01\,\mathrm{J/m}^2$, and $\gamma_{\omega\omega} = 0.022\,\mathrm{J/m}^2$. In this case, the ratio between interfacial energies is not high enough to counteract the strong thermodynamic (chemical) preference for the ω phase. As a result, the two ω variants tend to coalesce, rather than being separated by a β layer, as documented in Fig. 5. Despite the presence of interfacial energy penalties, the chemical driving force dominates, leading to direct contact between the ω variants. This confirms that the standard double-well model alone is insufficient to enforce separation under large ΔG.

A natural remedy might be to penalize the contact between the ω variants more strongly by increasing the ratio $\gamma_{\omega\omega}/\gamma_{\beta\omega}$. However, when $\ell_{\beta\omega} = \ell_{\omega\omega}$, the positive definiteness of the capillary matrix $\mathbb{H}$ imposes a strict bound: $\gamma_{\omega\omega} < 4\gamma_{\beta\omega}$ for $N = 2$, see (36). This bound limits our ability to enforce separation through energetic penalization. The restriction is severe: for example, if we attempt to simulate a case with $\gamma_{\omega\omega} = 5\gamma_{\beta\omega}$, the Newton solver fails to converge, and the finite element simulation crashes.

In a more general setting where $\ell_{\omega\omega} \neq \ell_{\beta\omega}$, the positive definiteness of the capillary matrix $\mathbb{H}$ requires a modified condition (see Appendix B), which seemingly allows the ratio of interfacial energies to be increased arbitrarily. However, as we now demonstrate, relaxing the equality of thicknesses leads to a violation of the EC condition and causes the simulation to produce unphysical results.

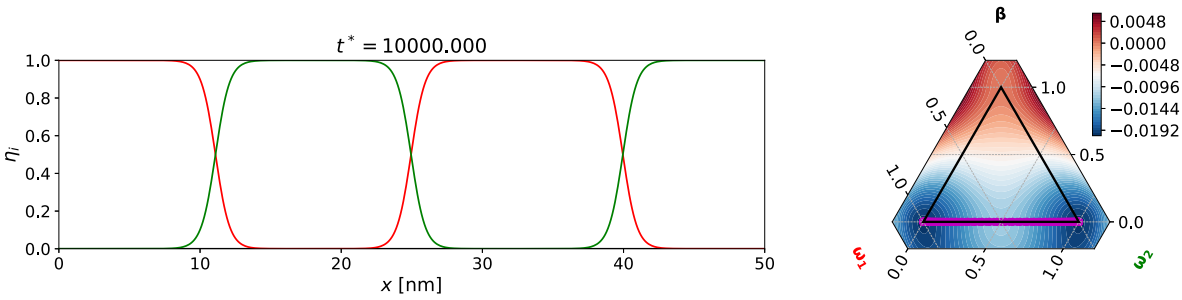

Fig. 5. Steady-state solution for $\Delta G = -0.02\,\mathrm{GPa}$, $\gamma_{\beta\omega} = 0.01\,\mathrm{J/m^2}$, and $\gamma_{\omega\omega} = 0.022\,\mathrm{J/m^2}$ using simple mixing. Phase fields η_0 (black), η_1 (red), and η_2 (green) are plotted across the domain. The ternary diagram on the right shows the corresponding composition points (magenta bullets). The strong chemical driving force causes the two ω variants to remain in direct contact, without an intermediate β phase. A video of the full simulation is available in the Supplementary material (see Movie M1).

8.3.2. *Documenting the importance of the EC condition for β–ω interfaces*

We now illustrate the practical significance of the EC condition. As discussed in Section 4, a somewhat counterintuitive but necessary requirement for EC in our model is the equality of interfacial thicknesses, i.e., $\ell_{\beta\omega} = \ell_{\omega\omega}$. To investigate the role of this condition, we intentionally violate it, thus violating the EC condition, and observe the consequences.

We use the same initial condition as in the previous case (see Fig. 4), but increase the interfacial energy $\gamma_{\omega\omega}$ by a factor of ten:

$$\gamma_{\beta\omega} = 0.01\,\mathrm{J/m^2}, \qquad \gamma_{\omega\omega} = 0.22\,\mathrm{J/m^2}, \tag{61}$$

and compensate for this increase by proportionally scaling the corresponding interfacial thicknesses:

$$\ell_{\beta\omega} = 1\,\mathrm{nm}, \qquad \ell_{\omega\omega} = 0.1\,\mathrm{nm}. \tag{62}$$

The simulation results are shown in Fig. 6. The top panel captures an early stage of the evolution at $t^* = 0.014$, where the order parameters temporarily drop below zero, violating the physical constraint $\eta_i \in [0, 1]$. This behavior highlights the importance of the EC condition in maintaining physically admissible solutions—its violation permits the system to diverge to non-physical regions of the energy landscape, including local minima outside the Gibbs simplex.

As the evolution proceeds, the system reaches a steady state at $t^* = 10000$ (bottom panel), which is spatially homogeneous and corresponds to a mixed composition strictly inside the simplex, lacking any pure-phase regions. The associated ternary diagrams (right-hand panels) confirm that the solution remains confined to an unseparated (mixed) state in composition space throughout the entire evolution.

These results demonstrate that failure to satisfy the EC condition can lead not only to transient violations of physical bounds (e.g., $\eta_i < 0$), but also to incorrect steady states characterized by the absence of proper phase separation.

While the effects of violating the EC condition may appear modest under weak chemical driving forces, we find its enforcement important for robust and physically consistent modeling of the considered process, particularly in regimes characterized by strong chemical driving or complex interfacial interactions. As shown in the next section, in some practically important cases, a moderate violation of EC resulting from simple chemical mixing can be compensated by sufficiently strong double-ditch augmentation of the energy functional.

8.3.3. *Comparing double-ditch model with simple vs. elliptic chemical mixing*

We will now compare the performance of the double-ditch augmented model in the two considered variants of chemical mixing – elliptic (satisfying EC) and simple (violating EC) – in a number of setups and using several error measures. We will show, in particular, that the lack of EC compliance of the simple mixing model can be partially compensated by strong enough double-ditch regularization.

EC condition compliance. We consider a one-dimensional test case, $N = 2$, with an initial condition consisting of a two-phase mixture of the β phase and the variant ω_1. The third phase, ω_2, is initially absent and should not appear during the simulation if the chemical energy formulation satisfies the EC condition. The initial condition is shown in Fig. 7. The initial condition includes a perturbation by a small-amplitude uniform noise. Note that η_2 is identically set to zero in the whole domain. The chemical energy is constant with a relatively large magnitude, $\Delta G = -0.02\,\mathrm{GPa}$, see e.g. Fig. 2.

We simulate the problem using two different chemical energy formulations: the simple mixing, which does not satisfy the EC condition, and the elliptic mixing, which is constructed to fulfill it. For both formulations, we vary the double-ditch parameter $\lambda \in \{0,\ 0.2,\ 5,\ 100\}\,\mathrm{GPa}$. To quantify the violation of the EC condition, we compute the average presence of ω_2 over time, measured by

$$\frac{1}{|\Omega|}\int_\Omega |\eta_2|\,\mathrm{d}x, \tag{63}$$

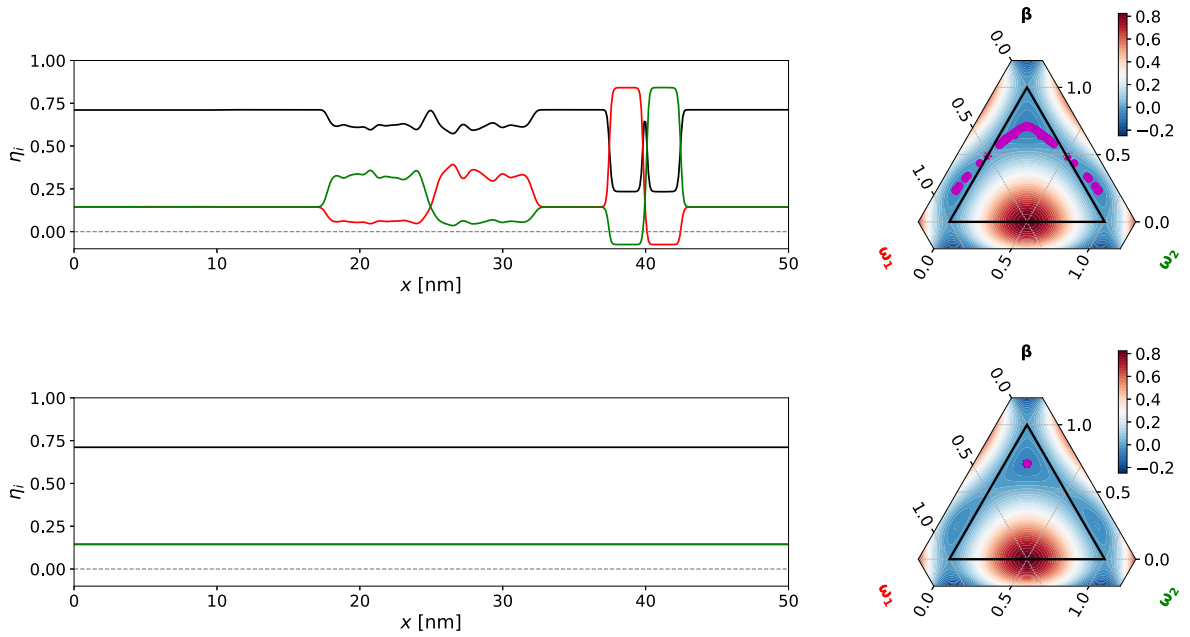

Fig. 6. Effect of violating the EC condition for β–ω interfaces. Results correspond to $\Delta G = -0.02\,\mathrm{GPa}$, $\gamma_{\beta\omega} = 0.01\,\mathrm{J/m^2}$, $\gamma_{\omega\omega} = 0.22\,\mathrm{J/m^2}$, with interfacial thicknesses $\ell_{\beta\omega} = 1\,\mathrm{nm}$ and $\ell_{\omega\omega} = 0.1\,\mathrm{nm}$, using simple chemical mixing. The top panel shows an intermediate state at $t^* = 0.014$, where the order parameters η_i temporarily fall outside the physical range. The bottom panel shows the steady-state solution at $t^* = 10000$, which is spatially uniform and corresponds to a fully mixed composition. In both cases, the ternary diagrams on the right display the corresponding composition points (magenta bullets). A video of the full simulation is available in the Supplementary material (see Movie M2).

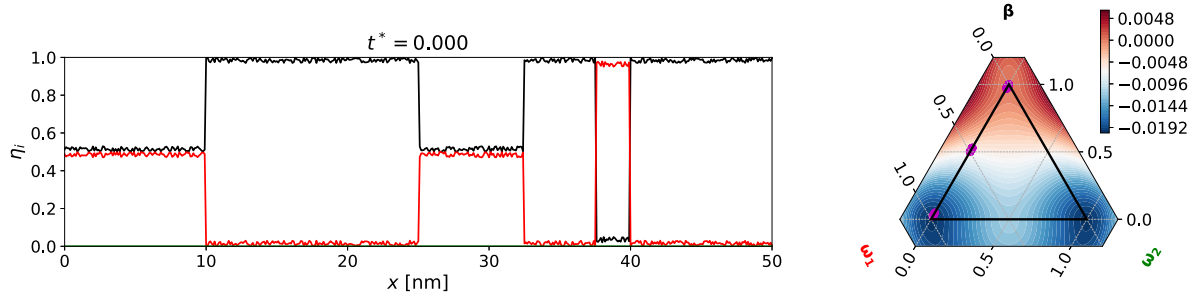

Fig. 7. Initial condition for the verification of the EC condition: the black curve represents η_0 and the red curve η_1. Only the β phase and the variant ω_1 are present; the variant ω_2 is absent and should remain so.

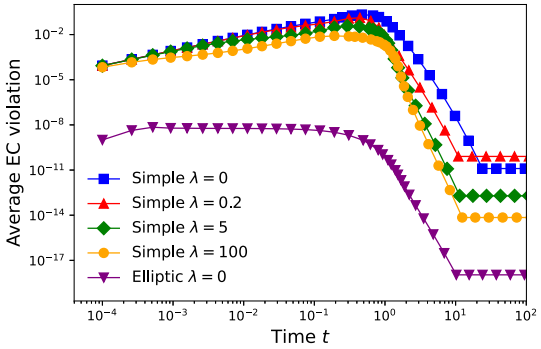

Fig. 8. Temporal evolution of the average EC violation, measured as $\frac{1}{|\Omega|}\int_\Omega |\eta_2|\,\mathrm{d}x$. The elliptic mixing shows a negligible violation during the initial stage caused by numerical round-off errors. For the simple mixing, the violation decreases with increasing regularization parameter λ.

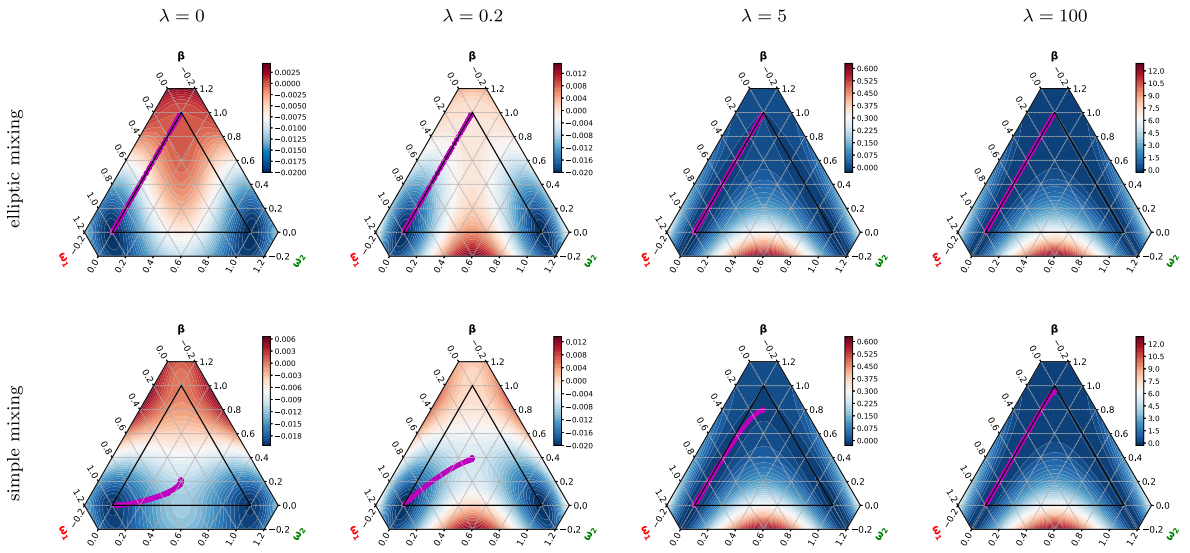

Fig. 9. Ternary plots at time $t^* = 0.5$ for different values of the double-ditch parameter λ, comparing elliptic mixing (top row) and simple mixing (bottom row). For the elliptic mixing, all points remain on the β–ω_1 edge, satisfying the EC condition. For the simple mixing, the deviation from the edge diminishes with increasing λ. Videos of the selected full simulation are available in the Supplementary material (see Movies M3a and M3b).

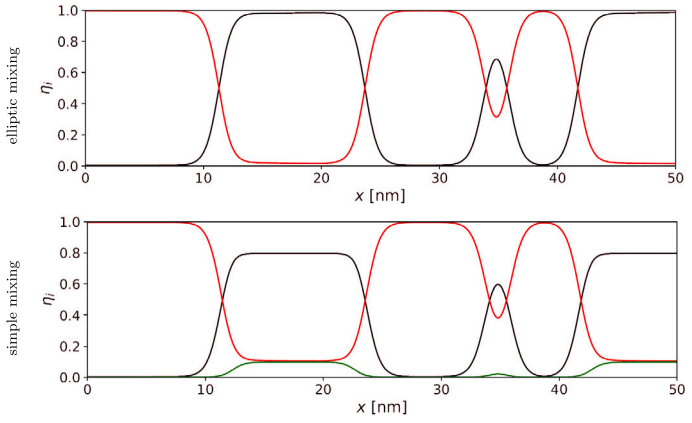

Fig. 10. Solution at time $t^* = 0.5$ for $\lambda = 5$ GPa, comparing elliptic mixing (top row) and simple mixing (bottom row). In the case of elliptic mixing, only the β phase (black line) and the ω_1 variant (red line) are present. For simple mixing, the ω_2 variant (green line) also appears, indicating that the EC condition is not satisfied.

as shown in Fig. 8. Interestingly, for the elliptic mixing, the average EC violation increases only during the first two time steps. In contrast, for the simple mixing, it increases for more than 20 time steps, regardless of the chosen double-ditch parameter λ.

To visualize the phase distributions, in Fig. 9, we present ternary plots at time $t^* = 0.5$ for both mixing types and for different values of λ. For the elliptic mixing (top row), all points lie along the β–ω_1 edge, indicating exact satisfaction of the EC condition (up to numerical precision). In contrast, the simple mixing (bottom row) leads to the spurious formation of ω_2, though this violation gradually diminishes as λ increases. The corresponding one-dimensional profiles for $\lambda = 5$ are shown in Fig. 10, where ω_2 appears only in the simple mixing case, documenting the violation of the EC condition.

Stability of the EC condition. We further examine the stability of the EC condition by introducing a small perturbation in the initial condition. Specifically, we slightly perturb the variant ω_2 such that η_2 is non-zero but remains close to zero at time $t^* = 0$. The goal is to test whether this small deviation from the β–ω_1 edge vanishes over time, i.e., whether the system naturally returns to the EC-compliant state. The perturbed initial condition is shown in Fig. 11.

The temporal evolution of the average EC violation given by Eq. (63) is plotted in Fig. 12. The results show that for both mixings the violation decays exponentially with time, indicating that the spurious ω_2 phase disappears. This behavior confirms the stability

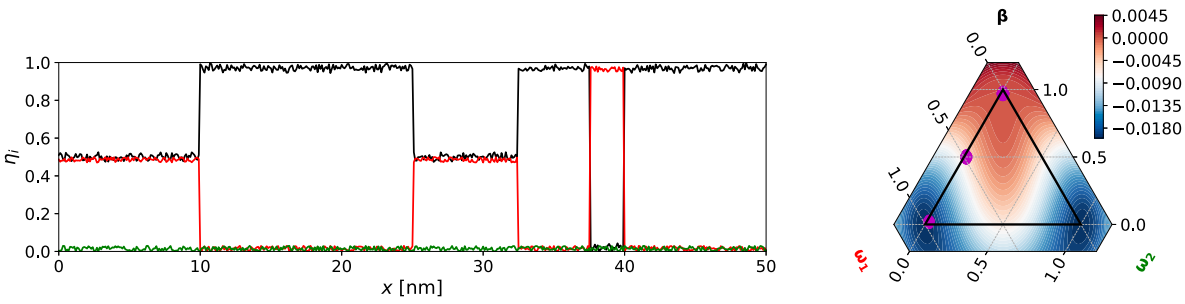

Fig. 11. Initial condition for the stability test of the EC condition: the black curve represents η_0, the red curve η_1, and the green curve η_2. The variant ω_2 is present with a small perturbation, i.e., $\eta_2 \approx 0$ but not identically zero.

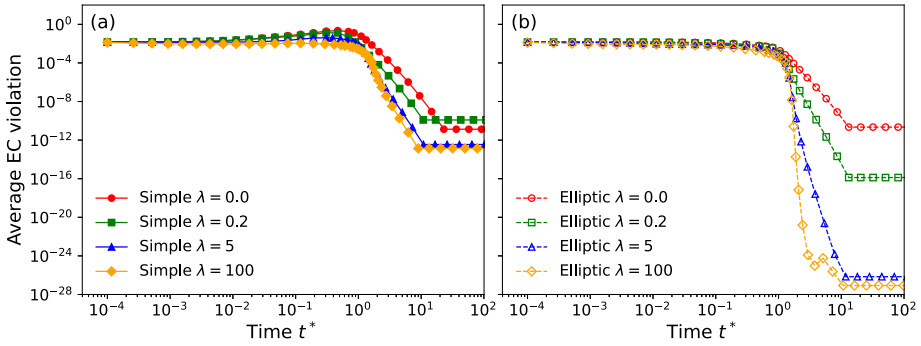

Fig. 12. Temporal evolution of the average EC violation for the test with a perturbed initial presence of ω_2, measured as $\frac{1}{|\Omega|}\int_\Omega |\eta_2|\,\mathrm{d}x$ for (a) simple and (b) elliptic mixing. The violation decays rapidly over time, indicating that the spurious variant ω_2 vanishes and the system returns to a physically consistent configuration.

of the EC condition: even if the initial state lies slightly off the β–ω_1 edge, the system quickly relaxes back to a physically consistent configuration, with $\eta_2 \to 0$.

Effect of the double-ditch parameter λ. As discussed in Section 6, for small values of the chemical energy difference ΔG, the standard double-well formulation without the double-ditch term may still yield acceptable results. However, when $|\Delta G|$ becomes larger, this formulation fails: the β phase disappears entirely and the two ω variants come into direct, undesired contact, cf. Fig. 5. To address this issue in a controlled way, we now fix $\Delta G = -0.02\,\mathrm{GPa}$ and vary only the double-ditch parameter λ.

The initial condition (see Fig. 4) consists of nearly pure phases of β, ω_1, and ω_2, with small random perturbations. It also contains phase mixtures such as β–ω_1 and β–ω_2, as well as ω_1–ω_2, the undesired contact of two ω variants.

The steady-state solutions for selected values of λ are shown in Figs. 13 and 14, using both the simple and elliptic mixing formulations. With $\lambda = 0$ and simple mixing, the β phase vanishes completely and the two ω variants are in direct contact (Fig. 13, top-left and Fig. 5). For elliptic mixing with $\lambda = 0$, the solution converges to a non-physical constant state with $\eta_0 = -5$ and $\eta_1 = \eta_2 = 3$ across the entire domain (outside the range of the ternary plots in Fig. 13). This unphysical behavior is due to a spurious minimum of the multiwell potential outside the Gibbs simplex in the total-spreading regime, as noted by (Boyer & Lapuerta, 2006). While this minimum exists for both mixing formulations, the elliptic model shifts the driving forces in such a way that the system can reach this state more readily, especially under weak or unstable initial conditions.

Introducing a small double-ditch penalty of $\lambda = 0.2\,\mathrm{GPa}$ is already sufficient to regularize the solution. A thin layer of the β phase reappears, separating the ω variants and eliminating the spurious minimum in both formulations. As λ increases further to 5 and 100 GPa, the separation becomes more robust, with a clearer and wider β phase forming between the ω variants. This separation with $\lambda = 100\,\mathrm{GPa}$ and both types of mixing is clearly visible in the spatial plots in Fig. 14.

8.4. Quinary system (N=4)

We now investigate a more complex quinary system involving four ω variants, extending our analysis to one-, two-, and three-dimensional settings.

8.4.1. 1D setting

For all simulations, we use $\Delta G = -0.02\,\mathrm{GPa}$, $\lambda = 100\,\mathrm{GPa}$, $\gamma_{\beta\omega} = 0.01\,\mathrm{J/m^2}$, and $\gamma_{\omega\omega} = 0.022\,\mathrm{J/m^2}$. As before, we first examine compliance with the EC condition.

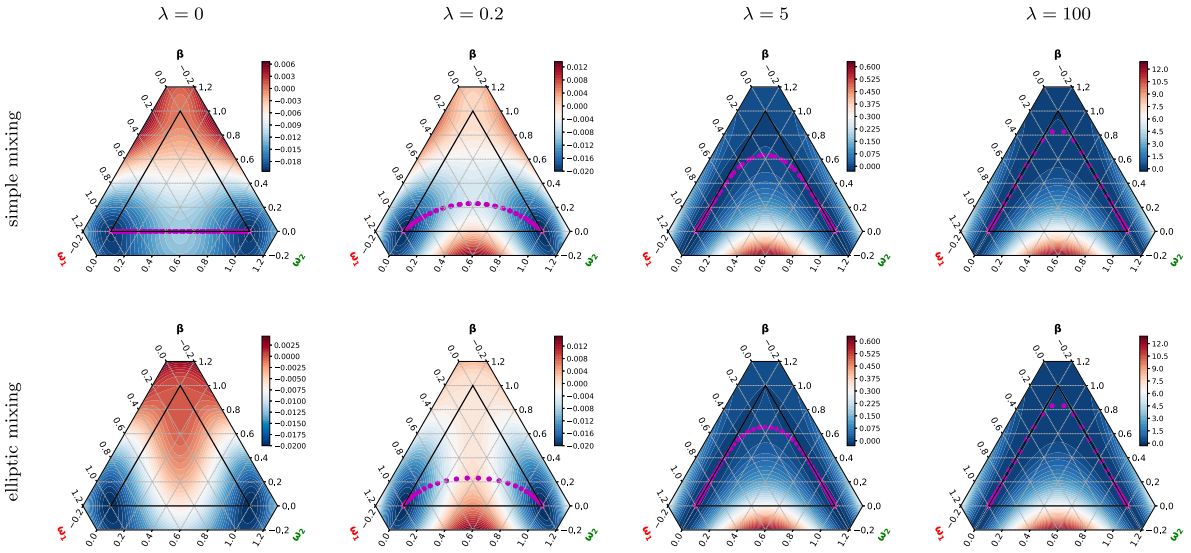

Fig. 13. Steady-state solutions for fixed $\Delta G = -0.02\,\mathrm{GPa}$ and varying double-ditch parameter λ. The initial condition is shown in Fig. 4. Each triangle shows the final composition points (magenta bullets) in the ternary diagram. Top row: simple mixing. Bottom row: elliptic mixing.

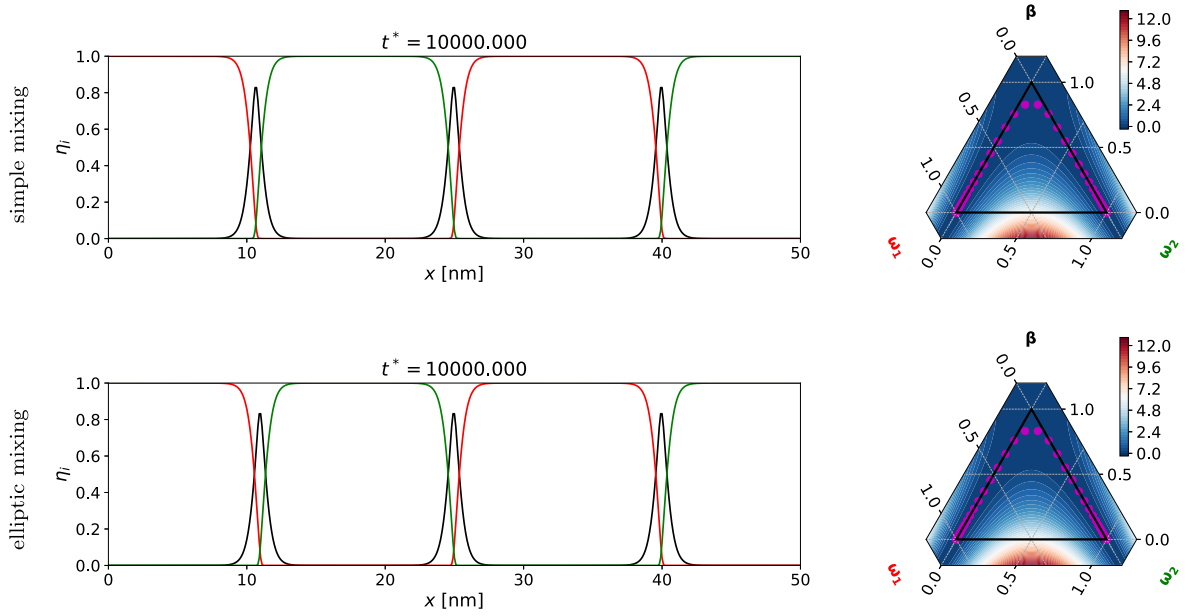

Fig. 14. Steady-state solutions for $\Delta G = -0.02\,\mathrm{GPa}$ and $\lambda = 100\,\mathrm{GPa}$. The spatial distribution of phases is shown using colors: η_0 (black), η_1 (red), and η_2 (green). Composition points are plotted in the ternary diagram as magenta bullets. The top row corresponds to simple mixing; the bottom row shows results for elliptic mixing. A video of the full simulation is available in the Supplementary material (see Movie M4).

EC condition compliance and stability. The initial condition is constructed similarly to Fig. 11—with only a single variant ω_1 present and the remaining ω variants initialized as small perturbations near zero. The specific configuration for the $N = 4$ system is shown in Fig. 15.

The evolution of the EC violation for η_2, η_3, and η_4 is shown in Fig. 16. Both simple and elliptic mixing exhibit a similar transient behavior, with violations stabilizing around 10^{-3} until $t^* \approx 2$. After that, the violations rapidly decrease. While the difference during the evolution is negligible, the elliptic formulation reaches significantly lower steady-state values, dropping below 10^{-28}, in contrast to about 10^{-14} for the simple mixing. This demonstrates that elliptic mixing leads to cleaner long-term solutions, although simple mixing already yields acceptable results.

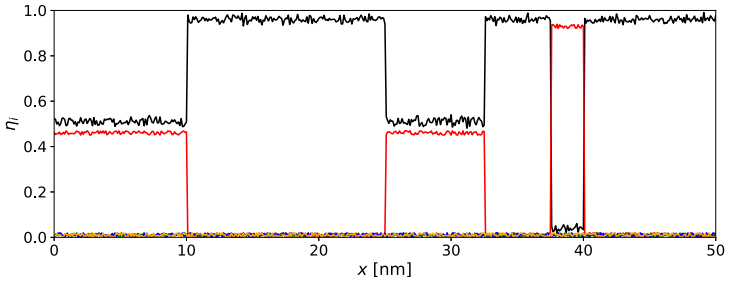

Fig. 15. Initial condition for the 1D EC compliance with $N = 4$. Initially, only η_1 is prescribed, η_2, η_3, and η_4 are perturbed close to zero. Phase fields: η_0 (black), η_1 (red), η_2 (green), η_3 (blue), η_4 (yellow).

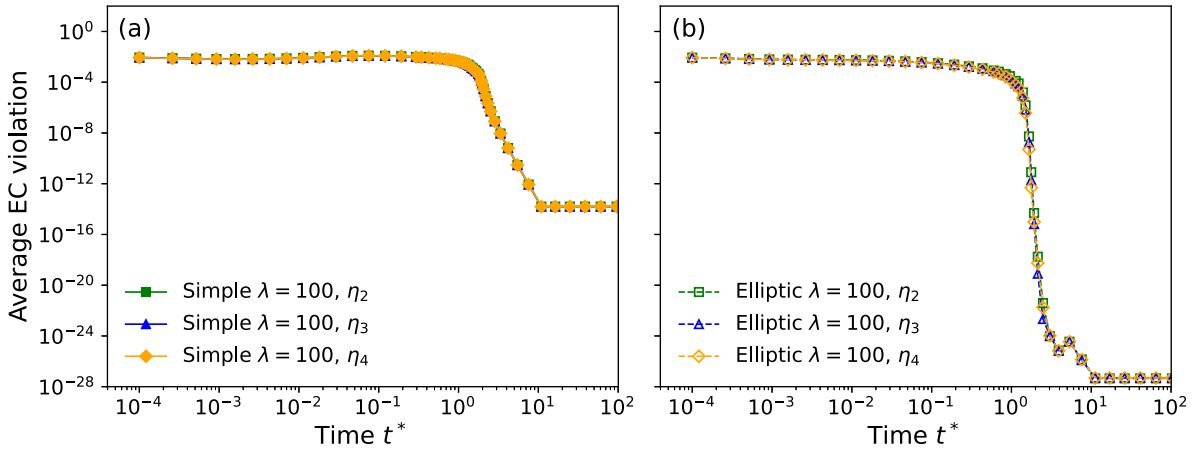

Fig. 16. EC violation for $N = 4$ and order parameters η_2, η_3, and η_4. The plot shows the average $\frac{1}{|\Omega|}\int_\Omega |\eta_i|\,\mathrm{d}x$ as a function of time for (a) simple and (b) elliptic mixing. Both formulations show similar behavior.

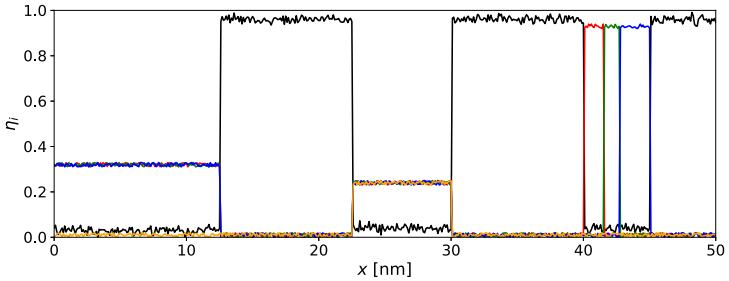

Fig. 17. Initial condition for the 1D simulation with $N = 4$, including all ω variants. Phase fields: η_0 (black), η_1 (red), η_2 (green), η_3 (blue), η_4 (yellow).

Simulation with all variants present. We now consider a simulation where all four ω variants are present in the initial condition. As shown in Fig. 17, the setup includes both ternary and quaternary mixtures, along with direct ω–ω interfaces.

The steady-state profiles are shown in Fig. 18 for both mixing models. In both cases, only ω_1 and ω_3 remain, separated by a layer of the β phase, demonstrating that the double-ditch penalty enforces proper separation of secondary phases.

We also monitor the interfacial, chemical and total free energies during the evolution. As shown in Fig. 19, the total free energy decreases monotonically in time for both mixing formulations; the same behavior is observed in higher-dimensional simulations.

During the evolution, we also check whether the physical constraint $0 \leq \eta_i \leq 1$ is satisfied. For both (simple and elliptic) formulations, the values never exceed one, but may drop occasionally below zero with the amplitude below 10^{-2}. Detailed time evolution of the error is provided in the Supplementary material, see Figure S1.

These 1D simulations confirm that the double-ditch works well to separate different ω variants by β phase even in the presence of four variants. Both mixing strategies lead to stable steady states with good EC compliance, and no unwanted variant formation. In the following sections, we extend the analysis to 2D and 3D simulations.

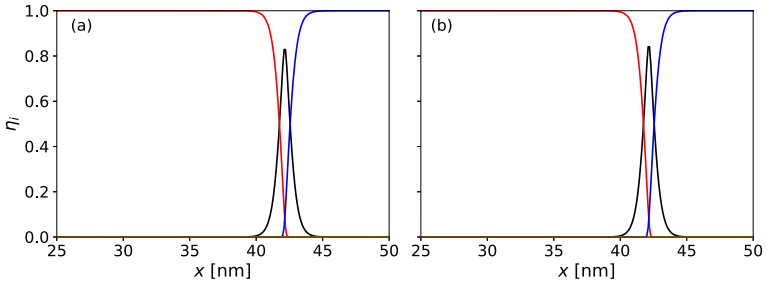

Fig. 18. Steady-state solutions for $\Delta G = -0.02\,\mathrm{GPa}$, $\lambda = 100\,\mathrm{GPa}$, and $N = 4$ using (a) simple and (b) elliptic mixing. Only ω_1 and ω_3 remain, separated by the β phase.

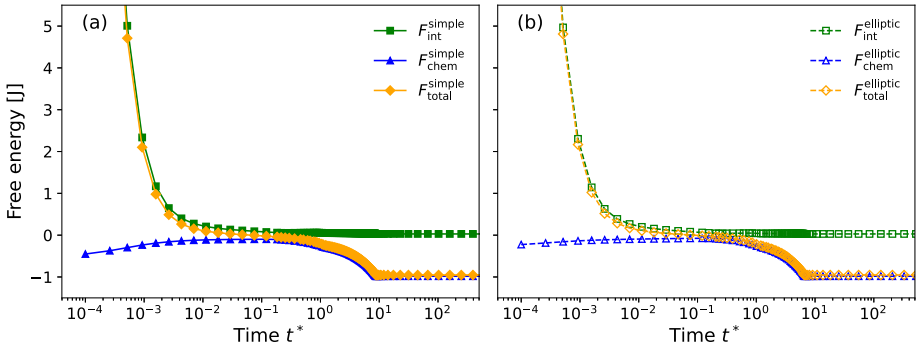

Fig. 19. Time evolution of the interfacial, chemical and total free energies for the one-dimensional simulation with $N = 4$ using (a) simple and (b) elliptic mixing. The total free energy decreases monotonically during the whole evolution.

8.4.2. 2D setting

We proceed with a two-dimensional numerical experiment to assess the behavior of the model with the double-ditch penalty ($\lambda = 100\,\mathrm{GPa}$) and elliptic mixing. As in the previous subsection, we set $\Delta G = -0.02\,\mathrm{GPa}$ and consider four ω variants. The initial condition, shown in the top-left panel of Fig. 20, consists of three ω variants – ω_1, ω_2, and ω_3 – placed in mutual contact. Small perturbations are added to all phase fields, resulting also in the presence of a minor amount of the fourth variant, ω_4. This setup allows us to observe whether any pathological behavior occurs near triple junction.

The domain is a square of size $50 \times 50\,\mathrm{nm}^2$, discretized using 256×256 quadrilateral elements. Periodic boundary conditions are applied in both spatial directions to reflect the intended physical setting of a domain embedded in a larger material domain.

A sequence of snapshots from the simulation is presented in Fig. 20. Shortly after the simulation begins, the β phase emerges between the initially present ω variants and separates them. As the system evolves, the three visible ω variants expand, followed by a coarsening process that ultimately leads to a steady state in which the domain is fully occupied by the ω_2 variant.

Similarly to the 1D setting, the physical constraint on the phase fields, $0 \leq \eta_i \leq 1$, is only mildly violated (maximal negative value of 0.0056 located within the interface regions), see also Figure S2 in Supplementary material.

8.4.3. 3D setting

Finally, we present a three-dimensional numerical simulation involving elliptic mixing and a double-ditch penalty parameter $\lambda = 100\,\mathrm{GPa}$. The chemical driving force is set to $\Delta G = -0.02\,\mathrm{GPa}$, and we consider four distinct ω variants.

As the initial condition, we impose a quadruple point configuration in which each ω variant initially occupies one of four symmetric regions that meet at the center of the domain, with planar interfaces between each pair of variants. The order parameters are not set to pure variant values but to intermediate values around 0.8, with small random noise added—not to trigger the evolution itself, but to break the symmetry and promote the development of possibly a more interesting solution. This initial condition is shown in the top-left panel of Fig. 21. The purpose of this setup is to investigate whether the ω variants become separated by parent β phase during the evolution.

The computational domain is a cube of size $50 \times 50 \times 50\,\mathrm{nm}^3$, discretized using $128 \times 128 \times 128$ cubes, each divided into six tetrahedra. Periodic boundary conditions are applied in all three spatial directions to mimic a representative volume element of a bulk material. The resulting system exceeds 8 million degrees of freedom and was solved on the Karolina supercomputer at the IT4Innovations National Supercomputing Center in Ostrava.

A sequence of snapshots from the simulation is shown in Fig. 21. Shortly after the start, all ω variants become separated by the β phase, similar to the behavior observed in the two-dimensional simulation. As the system evolves, the ω domains grow and then coarsen, as in the 2D case. Eventually, only a single variant, ω_3, remains and fills the entire domain in the steady state. Throughout

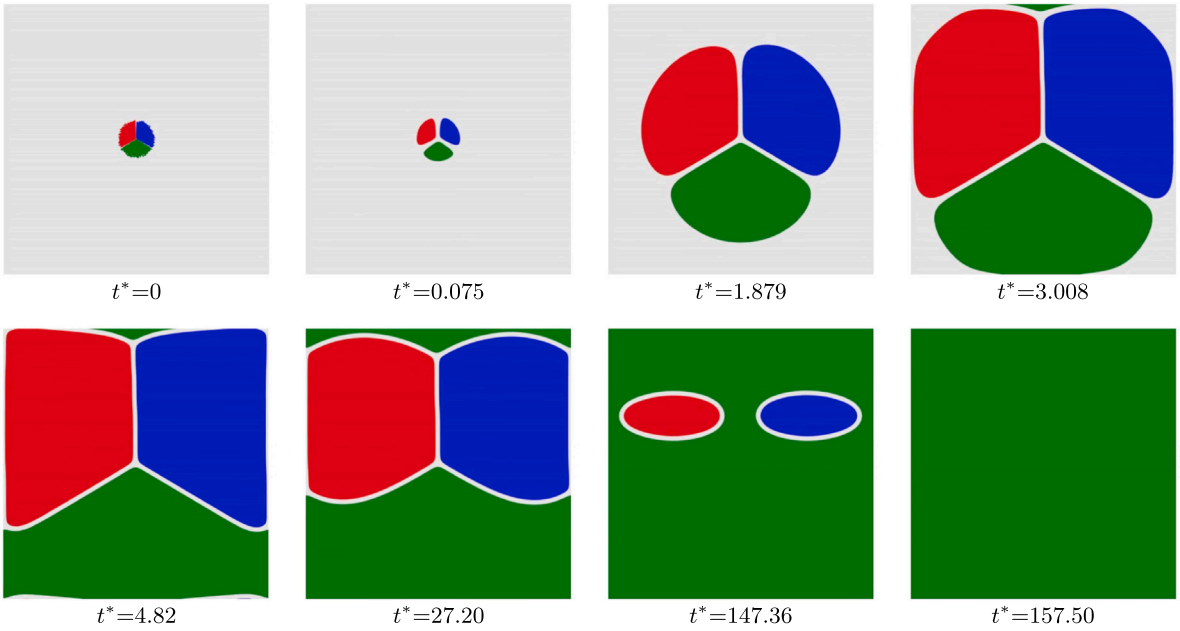

Fig. 20. Selected snapshots from the 2D simulation. The top-left panel shows the initial condition, while the subsequent images illustrate the system's temporal evolution up to the steady state, which is fully occupied by the ω_2 variant. The β phase is depicted in gray, and the ω variants are colored as follows: ω_1 in red, ω_2 in green, ω_3 in blue, and ω_4 in yellow (not visible). Each point is colored according to the variant ω_i for which the corresponding order parameter satisfies $\eta_i > 0.5$. A video of the full simulation is available in the Supplementary material (see Movie M5).

the simulation, the constraint on the order parameters $0 \leq \eta_i \leq 1$ is only slightly violated. The values always stay below one, but within the interfaces they can become slightly negative, with amplitudes smaller than 10^{-2}. The detailed time evolution of the error is shown in the Supplementary material, see Figure S3.

9. Discussion

Let us now briefly discuss some features of the model, in particular its connection to the published augmentations of the standard model (Boyer & Lapuerta, 2006), the implications of the EC condition for the freedom in choosing the mobility coefficients, and a summary comparison between the elliptic and standard chemical mixing approaches.

9.1. Relationship between the double-ditch augmentation and existing models

By introducing the double-ditch terms, we have extended the standard algebraic part of the multiwell potential with additional terms of the form $\lambda\eta_i^2\eta_j^2$. These off-diagonal terms, rejected by Boyer and Lapuerta (2006), are added selectively, only for the ω–ω pairs ($i, j \geq 1$). As shown in Section 6.1, the double-ditch augmentation preserves the EC condition for physically relevant two-phase β–ω states, while violating it only for the unphysical two-phase ω–ω states. This targeted violation is precisely the intended mechanism by which these spurious mixed ω–ω configurations are destabilized.

Specifically, in the ternary case comprising the β phase (η_0) and two ω variants (η_1, η_2), this augmentation takes the form $\lambda\eta_1^2\eta_2^2$. For comparison, in the same ternary setting, the following additional term in the free energy was proposed by Boyer and Lapuerta (2006) (see Eq. (38) therein):

$$\lambda\,\eta_0^2\eta_1^2\eta_2^2, \tag{64}$$

which we may refer to as a *triple-ditch* term. This penalization was originally introduced to eliminate non-physical minima of the multiwell potential that may arise outside the physically admissible region in the total-spreading regime. Numerical simulations reported by Boyer and Lapuerta (2006) demonstrate that a sufficiently large value of λ restores the non-negativity of the algebraic part of the free energy and constrains the evolution to remain within the physical range.

However, it is important to note that this augmentation does not allow relaxation of the condition (36) (Eq. (11) of Boyer and Lapuerta (2006)), which limits the allowable contrast in interfacial energies under total spreading. From this perspective, our double-ditch augmentation substantially broadens the regime of applicability of multiwell potential models.

Finally, we note that the triple-ditch term introduced by Boyer and Lapuerta (2006) – and its possible extensions to general multi-phase systems (cf. (Boyer & Minjeaud, 2014)) – could, in principle, be combined with the present double-ditch terms to suppress unphysical minima outside the Gibbs simplex and potentially further enhance model stability and convergence.

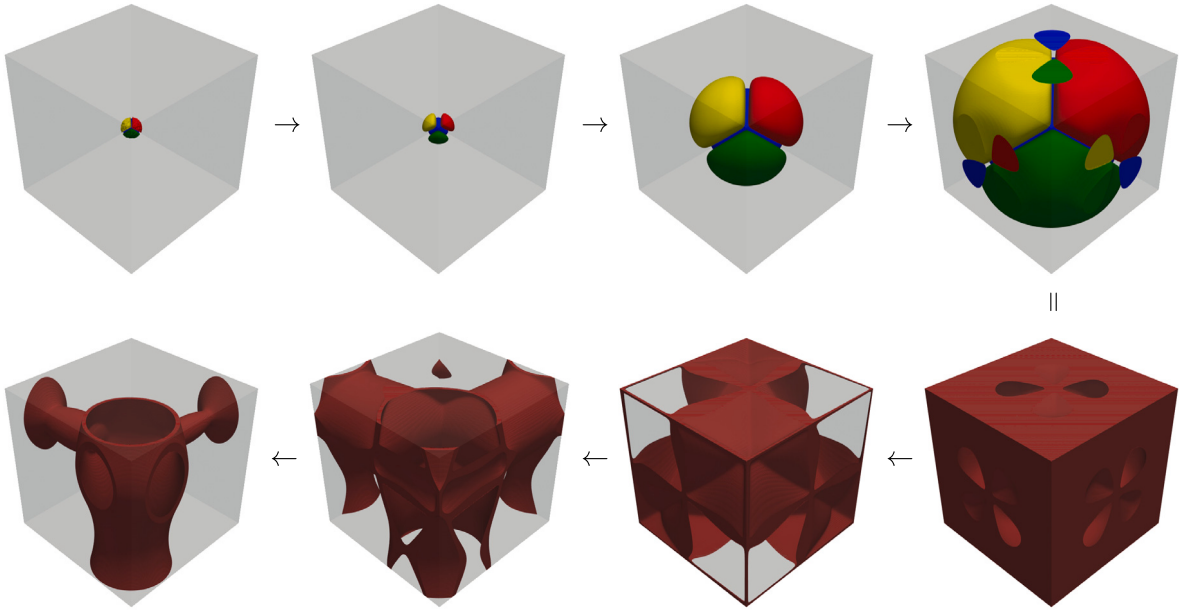

Fig. 21. Selected snapshots from the 3D simulation. The top-left panel shows the initial condition. The top row (left to right) depicts the evolution of the ω variants, colored as follows: ω_1 in red, ω_2 in green, ω_3 in blue, and ω_4 in yellow. The rightmost column shows both the ω variants (top) and the distribution of the β phase (bottom). The bottom row presents the subsequent evolution of the β phase, proceeding from right to left. The simulation eventually reaches a steady state fully occupied by ω_3 (not shown). Each point is assigned the color of ω_i if the corresponding order parameter satisfies $\eta_i > 0.5$. A video of the full simulation is available in the Supplementary material (see Movie M6).

9.2. Mobility coefficients

Let us now comment on the condition given in Eq. (28), which reads

$$m_\beta = M_\kappa \kappa_\beta^{-1}, \qquad m_\omega = M_\kappa \kappa_\omega^{-1},$$

linking the mobility coefficients m_β and m_ω to the capillary coefficients κ_β and κ_ω via a common scalar factor M_κ.

In the case of an interface separating two pure phases i and j, the *effective mobility* that governs the motion of the interface is given by $m_{ij} = m_i m_j/(m_i + m_j)$ (Rezaee-Hajidehi & Stupkiewicz, 2020). For a system with N equivalent ω variants, only two types of binary interfaces may arise: β–ω and ω–ω, with the corresponding effective mobilities

$$m_{\beta\omega} = \frac{m_\beta m_\omega}{m_\beta + m_\omega}, \qquad m_{\omega\omega} = \frac{m_\omega}{2}.$$

In our case, only one type of interfaces (β–ω interfaces) is physically relevant, while the other one (ω–ω interfaces) is not. Hence, it suffices to properly characterize the effective mobility of β–ω interfaces, $m_{\beta\omega} = m_\beta m_\omega/(m_\beta + m_\omega)$ (note that $m_{\beta\omega}$ is a physical parameter that can be measured experimentally, while m_β and m_ω are the model parameters). This can be achieved by adequately adjusting the two mobility parameters m_β and m_ω such that the condition (27) is also satisfied. This choice will imply an effective mobility of ω–ω interfaces, $m_{\omega\omega} = m_\omega/2$. However, those interfaces are to be ruled out by the phase-field model as non-physical, hence the corresponding mobility is irrelevant. The resulting explicit expressions for m_β and m_ω are thus given by

$$m_\beta = m_{\beta\omega}\left(1 + \frac{\kappa_\omega}{\kappa_\beta}\right), \qquad m_\omega = m_{\beta\omega}\left(1 + \frac{\kappa_\beta}{\kappa_\omega}\right). \tag{65}$$

Equivalently, this establishes a direct link between the effective mobility $m_{\beta\omega}$ and the proportionality factor M_κ as:

$$M_\kappa = (\kappa_\beta + \kappa_\omega) m_{\beta\omega}\ . \tag{66}$$

Thus, under our modeling assumptions, the constraint (28) still allows for arbitrary specification of the only physically meaningful mobility parameter, $m_{\beta\omega}$.

9.3. Comparison of simple and elliptic mixings: strengths and weaknesses

In Section 7, we have proposed a novel chemical mixing formulation with the goal of ensuring compliance with the EC condition even in simulations involving a chemical driving force. This goal has been partially achieved: we have identified an elliptic mixing expression that indeed satisfies the EC condition for β–ω interfaces.

However, a drawback emerges at ω–ω interfaces, where the elliptic mixing introduces a spurious thermodynamic driving force. This artifact necessitates at least a weak double-ditch regularization in case of elliptic chemical mixing. In the absence of such regularization (i.e., for $\lambda = 0$), simulations using elliptic mixing tend to converge to non-physical solutions outside the Gibbs simplex. Additionally, elliptic mixing introduces extra nonlinearity into the system, which slightly deteriorates numerical convergence.

By contrast, the standard simple mixing formulation, due to its violation of the EC condition, inherently introduces an artificial chemical preference among the ω variants. Interestingly, when combined with a sufficiently strong double-ditch augmentation, it performs reasonably well in numerical simulations and thus remains a viable modeling option.

While we opt for the more rigorous elliptic mixing formulation, the choice between elliptic and simple mixing may ultimately depend on the specific application and the balance between physical fidelity and numerical efficiency.

9.4. Possible extensions

In the present model, we have considered the interface energy augmented by a double-ditch term, which promotes the separation of different phases, together with a chemical energy contribution that distinguishes the thermodynamically preferred phase. A natural extension is to incorporate elastic energy, where the total strain is decomposed into elastic and transformational parts, the latter depending on the order parameters. The elastic energy then becomes a function of the elastic strain, with stiffness tensors varying with the order parameters so as to capture the anisotropic elasticity characteristic of the individual phases. Such an extension enables the description of a rich interplay between chemically driven growth and stress-mediated interactions, ultimately leading to the emergence of non-trivial microstructures. We plan to use this model in the framework of the $\beta \to \omega$ transformation in titanium alloys in a subsequent paper where spatially inhomogeneous concentration fields will be incorporated, as we believe this to be essential for any meaningful comparison with experimental observations.

10. Conclusions

In this work, we have proposed a novel augmentation of the standard multiwell model for phase separation in an $(N+1)$-component material consisting of one parent β phase and N variants of ω phases. The proposed formulation allows for a numerical treatment of cases with an arbitrarily large contrast in surface energies between ω–ω interfaces (total spreading regime), whereas in the standard model the maximum achievable contrast is limited to a relatively small value. We have demonstrated – both theoretically and through numerical simulations in one, two, and three spatial dimensions – that the new approach can efficiently mimic the crystallographic incompatibility of contact between selected phases (ω_i–ω_j, $i \neq j$) by introducing an energetic penalty.

The proposed multiwell model preserves the property of evolutionary consistency (EC), which ensures that purely two-phase β–ω_i states do not spontaneously evolve into configurations containing multiple ω variants. Furthermore, we have introduced a novel chemical energy mixing formula – termed *elliptic mixing* – which is compatible with the EC condition and reflects the chemical equivalence of the ω variants. We have systematically compared the performance of the standard and elliptic mixing formulations in a series of numerical experiments, highlighting the advantages of the proposed approach.

CRediT authorship contribution statement

J. Kozlík: Writing – review & editing, Writing – original draft, Visualization, Software, Methodology, Investigation, Conceptualization. **K. Tůma:** Writing – review & editing, Writing – original draft, Visualization, Supervision, Software, Resources, Methodology, Investigation, Conceptualization. **O. Souček:** Writing – review & editing, Writing – original draft, Methodology, Investigation, Conceptualization. **J. Dobrzański:** Writing – review & editing, Writing – original draft, Methodology, Investigation, Conceptualization. **S. Stupkiewicz:** Writing – review & editing, Writing – original draft, Supervision, Methodology, Investigation, Conceptualization.

Declaration of competing interest

The authors declare that they have no known competing financial interests or personal relationships that could have appeared to influence the work reported in this paper.

Acknowledgments

JK, KT and OS were supported by the Czech Science Foundation, Czechia, project No. 24-14578L (GAČR). JD and SS were supported by the National Science Centre (NCN) project No. 2022/47/I/ ST8/02879. KT and OS also acknowledge support from the Charles University Research Centre program, Czech Republic, No. UNCE/24/SCI/005, and are members of the Nečas Center for Mathematical Modeling. This work was further supported by the Ministry of Education, Youth and Sports of the Czech Republic through the e-INFRA CZ project (ID: 90254). We thank Prof. Yunzhi Wang (Ohio State University) for inspiring discussions that motivated the development of the model.

Appendix A. Equivalence of diagonal and off-diagonal forms of $\mathbb{H}$ and $\mathbb{M}$

In Section 3, the capillary matrix $\mathbb{H}$ has been adopted in a diagonal form, see Eq. (8). Considering that in our setting the N variants of the product ω phase are equivalent, matrix $\mathbb{H}$ is characterized by two parameters (κ_β and κ_ω, see Eq. (10)) and takes the form $\mathbb{H} = \mathrm{diag}(\kappa_\beta, \kappa_\omega, \dots, \kappa_\omega)$. Upon enforcing the sum-to-unity constraint, the reduced matrix $\hat{\mathbb{H}}$ is given by Eq. $(15)_2$.

An alternative way could be to adopt the capillary matrix $\tilde{\mathbb{H}}$ composed of only off-diagonal terms,

$$\tilde{\mathbb{H}} = \begin{bmatrix} 0 & \tilde{\kappa}_{\beta\omega} & \dots & \tilde{\kappa}_{\beta\omega} \\ \tilde{\kappa}_{\beta\omega} & 0 & \dots & \tilde{\kappa}_{\omega\omega} \\ \vdots & \vdots & \ddots & \vdots \\ \tilde{\kappa}_{\beta\omega} & \tilde{\kappa}_{\omega\omega} & \dots & 0 \end{bmatrix}, \tag{A.1}$$

characterized by two parameters $\tilde{\kappa}_{\beta\omega}$ and $\tilde{\kappa}_{\omega\omega}$ related to the β–ω_i and ω_i–ω_j interfaces, respectively. Imposing the sum-to-unity constraint $(1)_3$, the gradient part of the interfacial energy takes then the following form,

$$\nabla\boldsymbol{\eta} \cdot \tilde{\mathbb{H}}\, \nabla\boldsymbol{\eta}\Big|_{\nabla\eta_0 = -\sum_{i=1}^{N} \nabla\eta_i} = \nabla\hat{\boldsymbol{\eta}} \cdot \hat{\tilde{\mathbb{H}}}\, \nabla\hat{\boldsymbol{\eta}}, \tag{A.2}$$

with the corresponding reduced capillary matrix

$$\hat{\tilde{\mathbb{H}}} = -\tilde{\kappa}_{\omega\omega}\hat{\mathbb{I}} + (\tilde{\kappa}_{\omega\omega} - 2\tilde{\kappa}_{\beta\omega})\hat{\mathbf{1}} \otimes \hat{\mathbf{1}}. \tag{A.3}$$

The reduced capillary matrices $\hat{\mathbb{H}}$ and $\hat{\tilde{\mathbb{H}}}$, see Eqs. $(15)_2$ and (A.3), are equal when the two sets of coefficients satisfy the following relation:

$$\kappa_\beta = \tilde{\kappa}_{\omega\omega} - 2\tilde{\kappa}_{\beta\omega}, \qquad \kappa_\omega = -\tilde{\kappa}_{\omega\omega}. \tag{A.4}$$

This proves the equivalence of the diagonal and off-diagonal forms of the capillary matrix characterizing the gradient part of the interfacial energy in our special setting of N equivalent product phases.

Additionally, it can be checked that the above equivalence holds also for a capillary matrix composed of both diagonal and non-diagonal terms. Such a matrix would involve four coefficients, of which two would be redundant (linearly dependent), since the reduced matrix has only two distinct coefficients.

The above reasoning also holds for the dissipation potential and for the mobility matrix $\mathbb{M}$, see Eq. (12) (note that matrices $\mathbb{M}$ and $\mathbb{H}$ have the same structure). Accordingly, the diagonal and off-diagonal forms of the mobility matrix $\mathbb{M}$ are fully equivalent upon enforcing the sum-to-unity constraint.

Note that the equivalence of diagonal and off-diagonal forms discussed above does not hold in the general case of $N+1$ *distinct* phases when $N > 2$. The diagonal capillary matrix $\mathbb{H}$ involves then $N+1$ independent coefficients, while the off-diagonal matrix $\hat{\mathbb{H}}$ involves $\frac{1}{2}N(N+1)$ independent coefficients. For $N = 2$, the two numbers are equal and the equivalence holds.

Finally, it can be easily checked that, in the case of the double-well potential considered in this work, the equivalence of diagonal and off-diagonal forms does not hold for the algebraic part of the interfacial energy. Interestingly, it can be shown that, in the case of the double-obstacle potential (Steinbach, 2009), the equivalence holds also for the algebraic part, provided the N variants of the product phase are equivalent.

Appendix B. Conditions on the positive definiteness of the capillary matrix

The quadratic form $\nabla\hat{\boldsymbol{\eta}} \cdot \hat{\mathbb{H}}\, \nabla\hat{\boldsymbol{\eta}}$ given by Eq. $(13)_2$ is positive-definite if and only if the matrix $\hat{\mathbb{H}}$ is positive-definite. To check this, one can apply Sylvester's criterion, a necessary and sufficient condition stating that a matrix is positive-definite if and only if all leading principal minors are positive.

In the case of $N+1$ phases, the reduced capillary matrix has dimensions $N \times N$ and is of the form specified by Eq. $(15)_2$. Let $\hat{H}_j$ denote the jth leading principal minor of $\hat{\mathbb{H}}$. To ensure the positive definiteness of the matrix $\hat{\mathbb{H}}$, the following inequalities must hold,

$$\hat{H}_j > 0 \implies \kappa_\omega^{j-1}(j\kappa_\beta + \kappa_\omega) > 0, \qquad j = 1, \dots, N. \tag{B.1}$$

Since $\kappa_\omega > 0$ (cf. Eq. $(10)_2$), the general formula for the jth inequality takes the form

$$j\kappa_\beta + \kappa_\omega > 0. \tag{B.2}$$

Alternatively, after substituting Eq. (10), this leads to

$$\frac{2j}{j-1}\gamma_{\beta\omega}\ell_{\beta\omega} > \gamma_{\omega\omega}\ell_{\omega\omega}. \tag{B.3}$$

As the term $2j/(j-1)$ decreases as j increases, the principal leading minor of the highest order ($j = N$) determines the final restriction. Thus, the condition for the positive-definiteness of the reduced capillary matrix $\hat{\mathbb{H}}$ for $N+1$ phases is given by

$$\frac{2N}{N-1}\gamma_{\beta\omega}\ell_{\beta\omega} > \gamma_{\omega\omega}\ell_{\omega\omega}. \tag{B.4}$$

This condition, under the assumption $\ell_{\beta\omega} = \ell_{\omega\omega}$ (as follows from the EC condition, see Eq. (33)), yields the condition given in Eq. (36).

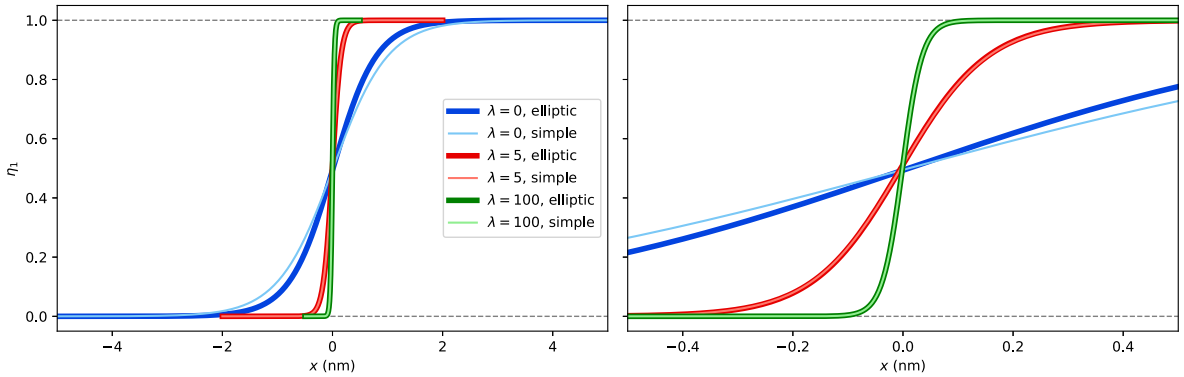

Fig. C.22. Profile of η_1 across a forced ω_1–ω_2 interface ($\eta_2 = 1-\eta_1$). Right: zoomed view of the central region. Minor differences are seen only for $\lambda = 0$; for larger λ, the two approaches yield nearly identical results.

Table C.1
Comparison of the effective interfacial energies $\gamma^{\mathrm{eff}}_{\omega\omega}$ (in $\mathrm{J/m^2}$) obtained from simulations using different mixing functions, alongside the theoretical prediction from Eq. (51).

λ	Mixing		$\gamma^{\mathrm{eff}}_{\omega\omega}$
	simple	elliptic	
0	0.0220	0.0278	0.0220
5	0.1372	0.1382	0.1372
100	0.6060	0.6062	0.6059

Appendix C. Effect of elliptic mixing on ω–ω interfacial energy

As noted in the main text, the elliptic mixing function is not constant along the ω–ω edge. Consequently, the assumptions used to derive Eq. (51) are no longer exactly satisfied. To quantify the potential error introduced by this inconsistency, we have conducted a series of one-dimensional numerical simulations of a forced ω_1–ω_2 interface in the absence of the β phase.

We compare the elliptic mixing function (58) against a reference case with constant chemical energy along the ω–ω edge, which corresponds to the simple mixing. Simulations were performed for three values of the regularization parameter λ, using the material parameters specified in Section 8.2 with $\Delta G = -0.02\,\mathrm{GPa}$.

The interfacial profiles are plotted in Fig. C.22. As shown, the difference between the two approaches is negligible for $\lambda = 5$ and 100 GPa. Only a small deviation is observed for $\lambda = 0$. The corresponding numerical values of the interfacial energies are summarized in Table C.1.

We conclude that although the elliptical mixing breaks the assumption of constant ω–ω chemical energy, the resulting error in interfacial energy is minor and becomes negligible for $\lambda \gtrsim 5\,\mathrm{GPa}$ with errors below 1%. In all practical simulations, this approximation is acceptable and does not compromise the validity of the model.

Appendix D. Supplementary data

Supplementary material related to this article can be found online at https://doi.org/10.1016/j.ijengsci.2026.104474.

Data availability

One-dimensional numerical results are available through a Zenodo repository: https://doi.org/10.5281/zenodo.16882290. The numerical results for 2D and 3D simulations will be shared upon request due to the repository size limitations.

References

Allen, S. M., & Cahn, J. W. (1979). A microscopic theory for antiphase boundary motion and its application to antiphase domain coarsening. *Acta Metallurgica, 27*(6), 1085–1095.

Ambati, M., Gerasimov, T., & Lorenzis, L. D. (2014). A review on phase-field models of brittle fracture and a new fast hybrid formulation. *Computational Mechanics, 55*(2), 383–405.

Banerjee, S., & Mukhopadhyay, P. (2007). *Phase transformations, volume 12: Examples from titanium and zirconium alloys* (1st ed.). Amsterdam ; Oxford: Elsevier Science.

Biben, T., Kassner, K., & Misbah, C. (2005). Phase-field approach to three-dimensional vesicle dynamics. *Physical Review E*, *72*(4).
Biot, M. A. (1965). *Mechanics of incremental deformations*. New York: John WIley & Sons Inc.
Bourdin, B., Francfort, G. A., & Marigo, J.-J. (2000). Numerical experiments in revisited brittle fracture. *Journal of the Mechanics and Physics of Solids*, *48*(4), 797–826.
Boyer, F., & Lapuerta, C. (2006). Study of a three component Cahn-Hilliard flow model. *ESAIM. Mathematical Modelling and Numerical Analysis*, *40*(4), 653–687.
Boyer, F., & Minjeaud, S. (2014). Hierarchy of consistent n-component Cahn–Hilliard systems. *Mathematical Models & Methods in Applied Sciences*, *24*(14), 2885–2928.
Caginalp, G. (1986). An analysis of a phase field model of a free boundary. *Archive for Rational Mechanics and Analysis*, *92*(3), 205–245.
Cahn, J. W., & Hilliard, J. E. (1958). Free energy of a nonuniform system. I. Interfacial free energy. *Journal of Chemical Physics*, *28*(2), 258–267.
Chen, L.-Q. (2002). Phase-field models for microstructure evolution. *Annual Review of Materials Research*, *32*(1), 113–140.
Chen, L.-Q., & Yang, W. (1994). Computer simulation of the domain dynamics of a quenched system with a large number of nonconserved order parameters: The grain-growth kinetics. *Physical Review B*, *50*(21), 15752–15756.
Choudhury, S., Li, Y. L., Krill III, C. E., & Chen, L.-Q. (2005). Phase-field simulation of polarization switching and domain evolution in ferroelectric polycrystals. *Acta Materialia*, *53*(20), 5313–5321.
Cook, H. E. (1975). On first-order structural phase transitions—II. The omega transformation in Zr-Nb alloys. *Acta Metallurgica*, *23*(9), 1041–1054.
Devaraj, A., Nag, S., Srinivasan, R., Williams, R. E. A., Banerjee, S., Banerjee, R., & Fraser, H. L. (2012). Experimental evidence of concurrent compositional and structural instabilities leading to ω precipitation in titanium–molybdenum alloys. *Acta Materialia*, *60*(2), 596–609.
Du, Q., Liu, C., & Wang, X. (2006). Simulating the deformation of vesicle membranes under elastic bending energy in three dimensions. *Journal of Computational Physics*, *212*(2), 757–777.
Ehemann, R. C., & Wilkins, J. W. (2017). Force-matched empirical potential for martensitic transitions and plastic deformation in Ti-Nb alloys. *Physical Review B*, *96*(18), Article 184105.
Fan, D., & Chen, L.-Q. (1997). Computer simulation of grain growth using a continuum field model. *Acta Materialia*, *45*(2), 611–622.
Gao, S., Liu, X., Lei, P., & Liu, W. (2025). Effects of high misfit on isothermal $\beta \rightarrow \omega$ phase transformation in Ti-19V alloy: A three-dimensional phase-field simulation. *Nuclear Engineering and Technology*, *57*(7), Article 103537.
Guin, L., & Kochmann, D. M. (2023). A phase-field model for ferroelectrics with general kinetics, part I: Model formulation. *Journal of the Mechanics and Physics of Solids*, *176*, Article 105301.
Halphen, B., & Nguyen, Q. (1975). Sur les matériaux standards généralises. *J. Mécanique*, *14*, 39–63.
Heida, M., Málek, J., & Rajagopal, K. R. (2012a). On the development and generalizations of Cahn–Hilliard equations within a thermodynamic framework. *Zeitschrift Für Angewandte Mathematik Und Physik*, *63*(1), 145–169.
Heida, M., Málek, J., & Rajagopal, K. R. (2012b). On the development and generalizations of Allen–Cahn and Stefan equations within a thermodynamic framework. *Zeitschrift Für Angewandte Mathematik Und Physik*, *63*(4), 759–776.
Kobayashi, R. (1993). Modeling and numerical simulations of dendritic crystal growth. *Physica D: Nonlinear Phenomena*, *63*(3–4), 410–423.
Levitas, V., & Preston, D. L. (2002). Three-dimensional Landau theory for multivariant stress-induced martensitic phase transformations. i. austenite↔martensite. *Physical Review B*, *66*, Article 134206.
Li, Y. L., Hu, S. Y., Liu, Z. K., & Chen, L.-Q. (2001). Phase-field model of domain structures in ferroelectric thin films. *Applied Physics Letters*, *78*(24), 3878–3880.
Miehe, C. (2011). A multi-field incremental variational framework for gradient-extended standard dissipative solids. *Journal of the Mechanics and Physics of Solids*, *59*, 898–923.
Moelans, N., Blanpain, B., & Wollants, P. (2008). An introduction to phase-field modeling of microstructure evolution. *Calphad*, *32*(2), 268–294.
Ode, M., Kim, S. G., & Suzuki, T. (2001). Mathematical modeling of iron and steel making processes. Recent advances in the phase-field model for solidification.. *ISIJ International*, *41*(10), 1076–1082.
Ohno, M., & Matsuura, K. (2010). Quantitative phase-field modeling for two-phase solidification process involving diffusion in the solid. *Acta Materialia*, *58*(17), 5749–5758.
Onsager, L. (1931). Reciprocal relations in irreversible processes. II.. *Physical Review*, *37*, 405–426.
Penrose, O., & Fife, P. C. (1990). Thermodynamically consistent models of phase-field type for the kinetic of phase transitions. *Physica D: Nonlinear Phenomena*, *43*(1), 44–62.
Rathgeber, F., Ham, D. A., Mitchell, L., Lange, M., Luporini, F., McRae, A. T., Bercea, G.-T., Markall, G. R., & Kelly, P. H. (2016). Firedrake: automating the finite element method by composing abstractions. *ACM Transactions on Mathematical Software (TOMS)*, *43*(3), 1–27.
Rezaee-Hajidehi, M., & Stupkiewicz, S. (2020). Phase-field modeling of multivariant martensitic microstructures and size effects in nano-indentation. *Mechanics of Materials*, *141*, Article 103267.
Singer-Loginova, I., & Singer, H. M. (2008). The phase field technique for modeling multiphase materials. *Reports on Progress in Physics*, *71*(10), Article 106501.
Šmilauerová, J., Harcuba, P., Kriegner, D., & Holý, V. (2017). On the completeness of the $\beta \rightarrow \omega$ transformation in metastable β titanium alloys. *Journal of Applied Crystallography*, *50*(1), 283–287, Publisher: International Union of Crystallography.
Steinbach, I. (2009). Phase-field models in materials science. *Modelling and Simulation in Materials Science and Engineering*, *17*, Article 073001.
Steinbach, I., & Pezzolla, F. (1999). A generalized field method for multiphase transformations using interface fields. *Physica D: Nonlinear Phenomena*, *134*(4), 385–393.
Steinbach, I., Pezzolla, F., Nestler, B., Seeßelberg, M., Prieler, R., Schmitz, G., & Rezende, J. (1996). A phase field concept for multiphase systems. *Physica D: Nonlinear Phenomena*, *94*(3), 135–147.
Tang, B., Cui, Y. W., Chang, H., Kou, H., Li, J., & Zhou, L. (2012). A phase-field approach to athermal $\beta \rightarrow \omega$ transformation. *Computational Materials Science*, *53*(1), 187–193.
Tang, B., Cui, Y. W., Kou, H., Chang, H., Li, J., & Zhou, L. (2012). Phase field modeling of isothermal $\beta \rightarrow \omega$ phase transformation in the Zr–Nb alloys. *Computational Materials Science*, *61*, 76–82.
Tůma, K., Rezaee-Hajidehi, M., Hron, J., Farrell, P., & Stupkiewicz, S. (2021). Phase-field modeling of multivariant martensitic transformation at finite-strain: Computational aspects and large-scale finite-element simulations. *Computer Methods in Applied Mechanics and Engineering*, *377*, Article 113705.
Ubachs, R. L. J. M., Schreurs, P. J. G., & Geers, M. G. D. (2004). A nonlocal diffuse interface model for microstructure evolution of tin–lead solder. *Journal of the Mechanics and Physics of Solids*, *52*(8), 1763–1792.
Wang, Y., & Khachaturyan, A. (1997). Three-dimensional field model and computer modeling of martensitic transformations. *Acta Materialia*, *45*, 759–773.
Wang, Y., & Li, J. (2010). Phase field modeling of defects and deformation. *Acta Materialia*, *58*, 1212–1235.
Wang, S.-L., Sekerka, R. F., Wheeler, A. A., Murray, B. T., Coriell, S. R., Braun, R., & McFadden (1993). Thermodynamically-consistent phase-field models for solidification. *Physica D: Nonlinear Phenomena*, *69*(1–2), 189–200.
Yan, J.-Y., & Olson, G. B. (2016). Computational thermodynamics and kinetics of displacive transformations in titanium-based alloys. *Journal of Alloys and Compounds*, *673*, 441–454.
Yeddu, H. K., & Lookman, T. (2015). Phase-field modeling of the beta to omega phase transformation in Zr–Nb alloys. *Materials Science and Engineering: A*, *634*, 46–54.
Zhang, J. X., & Chen, L.-Q. (2005). Phase-field microelasticity theory and micromagnetic simulations of domain structures in giant magnetostrictive materials. *Acta Materialia*, *53*(9), 2845–2855.
Zheng, Y., Banerjee, D., & Fraser, H. L. (2016). A nano-scale instability in the β phase of dilute Ti–Mo alloys. *Scripta Materialia*, *116*, 131–134.
Ziegler, H. (1963). Some extremum principles in irreversible thermodynamics with application to continuum mechanics. In I. N. Sneddon, & R. Hill (Eds.), *Progress in solid mechanics*: *Vol. IV*, Berlin, Heidelberg: Springer Verlag.